Regulation of the $G\alpha_q$ Signaling Pathway by Regulators of G Protein Signaling Proteins, G Protein-Coupled Receptor Kinase 2, and Small Molecule Inhibitors

by

David M. Thal

A dissertation submitted in partial fulfillment
of the requirements for the degree of
Doctor of Philosophy
(Chemical Biology)
in The University of Michigan
2010

Doctoral Committee:

Associate Professor John J.G. Tesmer, Chair
Professor Richard R. Neubig
Professor Anna K. Mapp
Assistant Professor Jason E. Gestwicki

To my parents

Acknowledgements

I would very much like to thank my advisor Dr. John “Big Crystals” Tesmer for all his support and guidance. I would like acknowledge his second semester biochemistry lectures at The University of Texas as part of the reason I decided to persue graduate school, for better or for worse. I am thankful to him for allowing me to rather naively join his lab with no real interest in protein crystallography. Yet, he was able to generate my current interest and appreciation for structural biology. I honestly don’t believe I could have had a better mentor.

I thank all my labmates for their support and for creating a fun work environment. I especially thank Dr. Aruna Shankaranarayanan for her guidance and support in my early stages as a graduate student, and for all of her many contributions to Chapter 2. I also thank Dr. Valerie Tesmer, Mark Nance, Cassie Boguth, and Dr. Chih-chin Huang for helping me during various stages of my work. I also thank Raymond Yeow and Emily Wu for their hardwork and contributions to Chapters 4 and 5. I would like to thank all the members of the Center for Chemical Genomics, and in particular, Martha Larsen for sharing her expertise and essentially teaching me everything I know in regards to high-throughput screening.

I thank all my committee members for their input and support. I especially thank Dr. Richard Neubig for not only sharing his technical expertise and lab resources; but for essentially acting as a co-mentor and teaching me the fundamentals of pharmacology. In addition, his enthusiasm for science is both relentless and inspiring, and I thank him for all the advice he has given me. I also thank all the lab members of the Neubig lab, in particular, Dr. Dave Roman for all his help with learning FCPIA.

I thank all of my Ann Arbor friends for making graduate school a very memorable and enjoyable experience. To Mike Steinbaugh, Matthew Molusky, Paul Moore, Levi Blazer, Ryan Evans, Dr. Dan Foster, Levi Blazer, Kelly Bakulski, Paul Marinec, Jennifer Massie, and the countless others, without you I wouldn't have enjoyed the fine experiences/traditions of football Saturdays, bowling Wednesdays, euchre domination, the Davezagon, Peyronie Pirates, ChemBio FTW, The Roaming Goats, Team Fit, and being kicked out of just about every bar Ann Arbor has to offer. I also thank my childhood friends Eric Johnson and Kristopher Garcia for their support over the years.

And finally and most importantly, I would like to thank both my parents and my sister for all their love and support. I especially thank my Mom who just recently received her PhD and has provided constant encouragement throughout.

Table of Contents

List of Figures

List of Tables

List of Abbreviations

Abl – abelson tyrosine kinase

AC – adenylyl cyclase

ADP – adenosine diphosphate

AF – Alexa Fluor

AGC – kinase group containing PKA, PKG, and PKC kinases

ANOVA – analysis of variance

ANS – 8-anilino-1-naphtalenesulfonic acid

ATP – adenosine triphosphate

B_2AR – beta(2)-adrenergic receptor

bGRK2 – biotin GRK2

bROS – bovine rod outer segments

BSA – bovine serum albumin

C13 – 51 nucleotide RNA aptamer specific for GRK2

cAMP – cyclic adenosine monophosphate

CCG – Center for Chemical Genomics (University of Michigan)

cGMP – cyclic guanosine monophosphate

CHAPS – 3-[(3-Cholamidopropyl)dimethylammonio]propanesulfonic acid

CMPD – compound

DAG – diacylglycerol

DH domain – Dbl homology domain

DMSO – dimethyl sulfoxide

DTT – dithiothreitol

FAM – 6-carboxyfluorescein

FCPIA – flow cytometry protein interaction assay

FP – fluorescence polarization

GAP – GTPase activating protein

GDP – guanosine diphosphate

GEF – guanine nucleotide exchange factor

GMPPnP - 5′-Guanylyl-imidodiphosphate

GPCR – G protein-coupled receptor

GRK – G protein-coupled receptor kinase

GRK2ct – c-terminal domain of GRK2

GTP – gaunosine triphosphate

GTPγS – guanosine 5'-O-[gamma-thio]triphosphate

HEPES – 4-(2-hydroxyethyl)-1-piperazineethanesulfonic acid

hGRK2 – human GRK2

HTS – high-throughput screening

IC_{50} – half maximal inhibitory concentration

IP_3 – inositol 1,4,5-trisphosphate

IPTG – Isopropyl β-D-1-thiogalactopyranoside

IRS-1 – insulin receptor substrate 1

JIP – JNK interacting protein

JNK – Jun N-terminal kinase

K_d – dissociation constant

K_i – inhibitory constant

Kir3 – inward rectifying potassium channel 3

K_m – Michaelis constant

LARG – leukemia associated RhoGEF

M_1AChR – M_1-muscarinic acetlycholine receptor

MAP kinase – mitogen-activated protein kinase

MBP – maltose binding protein

MCCSL– Medical Chemistry Core Synthesis Laboratory

MDM2 – murine double minute 2

MES – 2-(*N*-morpholino)ethanesulfonic acid

MFI – median fluorescent intensity

NFAT – nuclear factor of activated T-cells

MLSCN – Molecular Libraries Screening Centers Network

P-loop – phosphate binding loop

PCR – polymerase chain reaction

PDB – protein data bank

PDEγ - phosphodiesterase γ

PEG – polyethylene glycol

PH – pleckstrin homology domain

PI3K – phosphoinositide 3-kinase

PIP_2 – phosphatidylinositol 4,5-bisphosphate

PKA – cAMP dependent protein kinase

PKC – protein kinase C

PKG – cGMP dependent protein kinase

PLCβ – beta isoforms of phospholipase

PLK-1 – polo-like kinase 1

PPI – protein-protein interaction

PPII – protein-protein interaction inhibitor

RGS – regulator of G protein signaling

RH domain – RGS homology domain

rrmsd – root mean square deviation

ROK – Rho associated serine/threonine kinase

SEM - Standard Error of Measurement

S/N – signal-to-noise ratio

SD – standard deviation

SDS-PAGE – sodium dodecyl sulfate polyacrylamide electrophoresis

TEV – tobacco etch virus

T_m – melting temperature

UM - University of Michigan

UNM – University of New Mexico

Abstract

Transmembrane signaling through $G\alpha_q$-coupled receptors is linked to physiological processes such as cardiovascular development and smooth muscle function. Crystallographic studies have shown that $G\alpha_q$ forms an effector like interaction with G protein-coupled receptor kinase 2 (GRK2) in a manner that does not appear to sterically overlap with the binding site for regulators of G protein signaling (RGS) proteins. We confirm the formation of higher order RGS-$G\alpha_q$-effector complexes using a flow cytometry protein interaction assay (FCPIA). Our data further supports the notion that GRK2 is a *bona fide* effector of $G\alpha_q$.

Indeed, protein interactions involving GRK2 have become increasingly complex. There is growing evidence that GRK2 phosphorylates many non-GPCR substrates, some of which are in response to activation of $G\alpha_q$-coupled receptors. Small molecule inhibitors that could specifically inhibit the binding of $G\alpha_q$ to GRK2 would serve as powerful pharmacological tools that could be used to better understand the full significance of this interaction. We developed a high-throughput screening assay using FCPIA to identify small molecule inhibitors of the $G\alpha_q$-GRK2 interaction. While our initial screening efforts failed to yield any discernable lead compounds, modifications of our assay could be used

to screen additional chemical libraries that are better designed towards inhibiting protein-protein interactions.

The canonical role of GRK2 is to phosphorylate the cytoplasmic tails/loops of activated G protein-coupled receptors (GPCRs). Phosphorylated receptors can then be uncoupled from G proteins, thereby desensitizing the signaling pathway. Since the discovery of a linkage between the over-expression of GRK2 and heart failure, GRK2 has become a pharmaceutical target for the treatment of heart disease. Takeda Pharmaceuticals have discovered a class of selective GRK2 inhibitors. We have solved the crystal structures of two of these compounds bound to GRK2-G$\beta\gamma$. Our crystal structures reveal that these compounds bind to an inactive kinase conformation, in a manner similar to the cancer drug imatinib. Recently, an RNA aptamer has been discovered that is also capable of selectively inhibiting GRK2. Crystallographic data indicates that the aptamer stabilizes an inactive conformation similar to that recognized by the Takeda compounds. We have developed an aptamer displacement assay using FCPIA that is currently in use to screen for small molecule inhibitors that bind to this inactive kinase conformation.

Chapter 1
General Introduction

G Protein-Coupled Receptor Signaling

Cell to cell communication is an essential process for all forms of life. Signal transduction is the cellular mechanism whereby environmental stimuli are converted into specific cellular responses. At the hub of signal transduction pathways are cell surface receptors, which receive extracellular signals (such as light, odors, hormones, etc.) as an input and output intracellular signals that affect physiological processes ranging from vision, taste, and smell to neurotransmission, blood pressure, and immune response. One class of cell-surface receptors is the G protein-coupled receptors (GPCRs), which are a family of integral membrane proteins that contain seven-transmembrane spanning helices. GPCRs are involved in a wide variety of both physiological and pathophysiological processes. They are a major pharmaceutical target and account for 30-60% of all modern drugs (*1-4*).

GPCRs constitute the largest superfamily of cell surface receptors and are comprised of over 800 genes (~4% of total human genes) (*5*). They are only found in eukaryotes, and are present in yeast, plants, protozoa, and metazoa (*1*). Structurally, GPCRs can be characterized by an extracellular N-terminus,

followed by seven transmembrane α-helices that form three intracellular loops and three extracellular loops, and an intracellular C-terminus (*6*). The GPCR superfamily has classically been divided into three main families (A, B, and C) based on protein sequence similarity (*7*). Family A is the largest member accounting for approximately 90% of all GPCRs with rhodopsin being the prototypical member. A characteristic feature of family A GPCRs is a conserved DRY sequence motif in the cytoplasmic end of 3rd transmembrane domain, which plays an important role in regulating conformational states (*8*).

GPCRs are given their name for their ability to activate heterotrimeric GTP-binding proteins (G proteins), which are composed of α, β, and γ subunits. G proteins serve as molecular switches by coupling the activation of a receptor to an intracellular response. In the inactive state, G proteins form a heterotrimer where Gα binds GDP and a constitutive Gβγ heterodimer. Upon receptor activation, GPCRs act as guanine-nucleotide exchange factors (GEFs) and promote the dissociation of GDP from the Gα subunit, allowing GTP to bind, and causing dissociation of the Gα-GTP and Gβγ subunits (Figure 1). Activated Gα-GTP and free Gβγ subunits are then able to bind their respective effector molecules and initiate downstream signaling pathways such as the cyclic adenosine monophosphate (cAMP) pathway and the phosphotidylinositol pathway (*9*). The signaling pathway is terminated when the Gα subunit hydrolyzes GTP to GDP, causing the reassociation of Gα-GDP and Gβγ into the inactive heterotrimeric G protein. The termination process can be accelerated by

GTPase activating proteins (GAPs) such as regulator of G protein signaling (RGS) proteins, which enhance the intrinsic GTPase activity of most Gα subunits (*4, 10-12*).

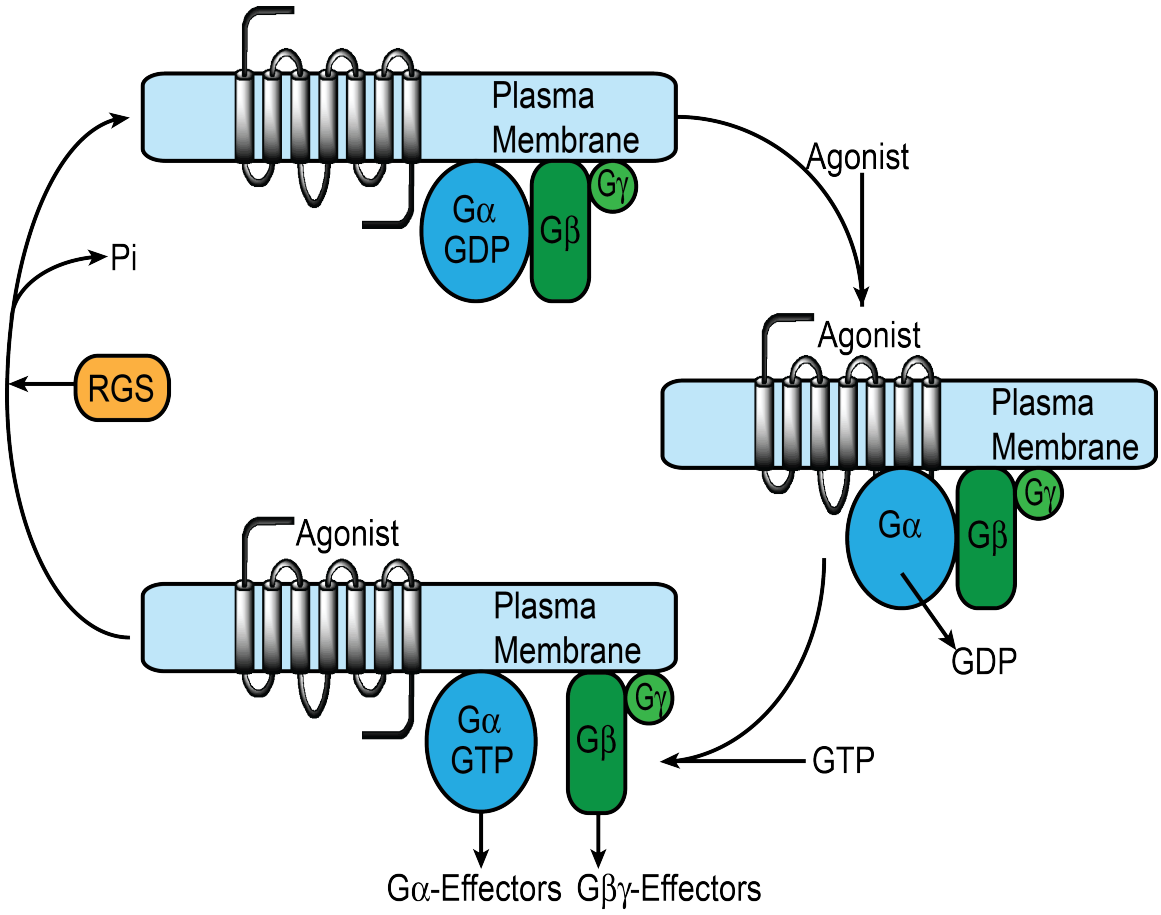

Figure 1: Canonical GPCR signaling pathway. Upon agonist binding, the GPCR becomes activated and catalyzes the exchange of GTP for GDP on the Gα subunit, activating both the Gα and Gβγ subunits. Gα-GTP and Gβγ are then free to bind and activate their respective effector molecules, which then generate second messenger molecules and continue the signaling cascade. Signaling is terminated when GTP is hydrolyzed to GDP by intrinsic GTPase activity of the Gα subunit.

In addition to activating G proteins, the activation of GPCRs triggers their phosphorylation by G protein-coupled receptor kinases (GRKs). In a process termed homologous desensitization, phosphorylated receptors are bound by a family of proteins called arrestins that block coupling with heterotrimeric G proteins. Arrestins can also induce receptor downregulation by coupling phosphorylated receptors to the endocytic machinery to internalize receptors (*13-15*).

Structure and Function of Heterotrimeric G proteins

Whereas there are over 800 GPCRs, there are relatively few heterotrimeric G proteins. There are 21 $G\alpha$ subunits (encoded by 16 genes), five $G\beta$ subunits, and 12 $G\gamma$ subunits. $G\alpha$ proteins are divided into four main classes based on primary sequence identity between the $G\alpha$ subunits: $G\alpha_s$, $G\alpha_i$, $G\alpha_q$, and $G\alpha_{12/13}$ (*11*). In the active, GTP-bound state, $G\alpha$ subunits bind and activate specific effector proteins, with each class of $G\alpha$ subunits traditionally linked to one or more specific effector proteins. For example, activated $G\alpha_s$ stimulates adenylyl cyclase (AC) resulting in an increase of the second messenger cAMP, whereas activated $G\alpha_i$ inhibits production of cAMP from AC. Activated $G\alpha_q$ activates phospholipase C-β (PLCβ) which cleaves the phospholipid phosphatidylinositol 4,5-bisphosphate (PIP_2) into diacyl glycerol (DAG) and inositol 1,4,5-triphosphate (IP_3). $G\alpha_{12/13}$ subunits activate Rho guanine nucleotide exchange factors (RhoGEFs) which further activate small GTPases such as RhoA. Furthermore,

free Gβγ subunits can activate a number of effectors such as PLCβs, ACs, phosphitidylinositide 3-kinase (PI3K), inwardly rectifying potassium channels, and voltage-gated calcium channels (*11, 16*).

The Gα Subunit

Structurally, Gα subunits are composed of two domains: a GTPase domain involved with the binding and hydrolysis of GTP, and an α-helical domain that forms a lid over the nucleotide binding site (Figure 2). The GTPase domain belongs to the Ras GTPase superfamily and is composed of a six-stranded β-sheet surrounded by five α-helices. The most highly conserved sequences in this domain are those used in guanine nucleotide binding: the diphosphate (P) loop (GXGESGKS), the Mg^{2+}binding loops (RXXTXGI and DXXG), and the guanine nucleotide binding motifs (NKXD and TCAT). This domain is typically known for the three flexible loops near the γ-phosphate binding site termed switches I, II, and III, which show significant structural differences between the GDP- and GTP-bound forms (Figure 2A). Switch I contains the Mg^{2+} binding loop, which participates in GTP hydrolysis along with the P loop, and its structure is only slightly affected by GTP hydrolysis or effector/regulator protein binding. Switch II also contributes to the hydrolysis of GTP, and forms part of the binding pocket for the γ-phosphate from GTP. Upon GTP hydrolysis switch II transitions from a more ordered to a less ordered conformation (Figure 2B). Switch III is a loop that contacts switch II through ionic and polar interactions in the GTP-bound

state. Overall, the loss of stability in switches II due the GDP bound state is responsible for the change in affinity of Gα subunits for effectors (*16-18*).

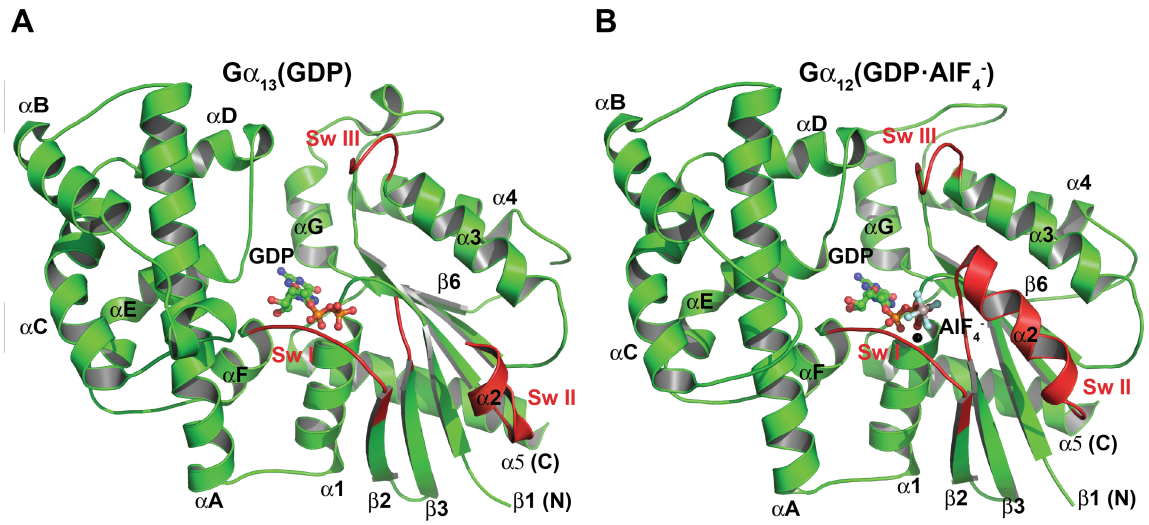

Figure 2: Crystal structures of $G\alpha_{12/13}$ in the deactivated and activated states. The secondary structural elements for the α-helical domain are labeled with letters (e.g. αA) and the GTPase domain are labeled with numbers (e.g. α1 and β2). The three flexible switch regions that undergo a conformational change upon nucleotide exchange are colored in red. The GDP and Mg^{2+}·GDP·AlF_4^- ligands bind in the active site and are shown as a ball and stick models with carbons colored green, nitrogens blue, oxygens red, phosphates orange, aluminum peach, fluorines white, and magnesium black. **A)** The inactive $G\alpha_{i/13}$·GDP complex (PDB:1ZCB) in a open conformation. Switch II is completely disordered and switch III is rotated away from the nucleotide-binding site. **B)** The activated $G\alpha_{i/12}$·GDP·AlF_4^- complex (PDB:1ZCA) in a closed conformation. Switch II is now ordered and switch III is closer to the nucleotide-binding site,

thus forming an interface between the α2 and α3 helices that bracket the effector-binding site.

The Gβγ Subunits

The G protein β and γ subunits form a constitutive dimer that cannot be dissociated except by denaturation. Gβ has a seven-bladed β-propeller structure that is formed by seven WD40 repeats, with each repeat being composed of four antiparallel β-strands. The Gβ subunit interacts with both the switch I and II regions of the GDP-bound Gα subunit and the N-terminal helix of the Gα subunit. The Gγ subunit is small protein (~8 kDa) consisting of two α-helices that form a coiled coil with the N terminal helical segment of Gβ. All Gγ subunits undergo a posttranslational lipid modification at their C-termini consisting of either a 15-carbon farnesyl or 20-carbon geranylgeranyl group (*11*).

$G\alpha_q$ Signaling and its Physiological Roles

The heterotrimeric G protein G_q is a key regulator of cardiovascular development and function (*20*). Approximately 40% of all GPCRs couple to the G_q family of Gα subunits, which consists of four members: $G\alpha_q$, $G\alpha_{11}$, $G\alpha_{14}$, and $G\alpha_{15/16}$. The canonical effectors for all G_q family members are the β-isoforms of PLC, which hydrolyze PIP_2 into IP_3 and DAG (*19*). These second messengers propagate and amplify the G_q-mediated signal by releasing intracellular stores of calcium and activating protein kinase C (PKC). Together, inosititol lipids, DAG, PKC, and

calcium are able participate in multiple signaling networks linking G_q-coupled receptors to a wide range of physiological functions such as cell growth and proliferation, platelet aggregation (*20*), neuronal signaling, glucose secretion, actin cytoskeleton reorganization (*21*), and smooth muscle contraction (*19, 22, 23*).

In addition to interacting with PLCβ, G_q family members interact with a myriad of other binding partners. In particular, activated $G\alpha_q$ has been show to bind to the guanine nucleotide exchange factor, p63RhoGEF (*24*), which activates the small G protein RhoA. Furthermore, activated $G\alpha_q$ has been shown to bind to: G protein coupled receptor kinase 2 (GRK2 (*25-28*) and GRK3 (*29*)), non-receptor guanine nucleotide exchange factor Ric-8A (*30, 31*), tubulin (*32, 33*), caveolin-1 (*34*), non-receptor tyrosine kinase Btk (*35*), and the p110α subunit of PI3K (*36*). Thus, overall signaling through $G\alpha_q$ is fairly complex, as one might expect for a protein that is involved in such a wide range of physiological functions.

While all G_q family members share the common effector PLCβ, they are not functionally redundant, and differ in tissue expression, amino acid sequence identity, downstream binding partners, and ultimately cell physiology. $G\alpha_q$ and $G\alpha_{11}$ are ubiquitously expressed and have a 90% amino acid sequence identity. $G\alpha_{14}$ is expressed in the kidney, liver, and lung, and is 80% similar in amino acid sequence identity with respect to $G\alpha_q$, and $G\alpha_{15/16}$ is found only in tissues rich in hematopoietic cells, where it plays an important role in erythroid differentiation

and T-cell activation. Both $G\alpha_q$ and $G\alpha_{11}$ are dually palmitoylated at cysteines Cys9 and Cys10, which has been shown to be important for membrane attachment and interactions with proteins and lipids. Furthermore, the N-terminal region is highly positively charged and contains contact residues for $G\beta\gamma$ subunits, making the N-terminal region critical for G protein function (*19*).

Genetic studies of $G\alpha_q$ have heavily implicated $G\alpha_q$ signaling in the development of heart failure (*19, 37*). Double homozygous null mutations for $G\alpha_q$ and $G\alpha_{11}$ induce cardiomyocyte hypoplasia and embryonic lethality, while mice with one intact allele of either gene die shortly after birth due to cardiac defects (*38*). Selective disruption of $G\alpha_q$ impairs platelet function and increases bleeding times in mice (*20, 39*). Further studies with transgenic cardiomyocyte lines prove that $G\alpha_q$ is essential for cardiomyocyte hypertrophy and proliferation during development, and link $G\alpha_q$ signaling to cardiac hypertrophy and heart failure in adults (*38, 40*). Additionally, loss of $G\alpha_q$ affects neuronal cerebellar activity (*41*) and impairs lung function in response to allergens (*42*). In contrast to $G\alpha_q$, mice genetically deficient in $G\alpha_{11}$, $G\alpha_{14,}$ and $G\alpha_{15}$ show normal growth characteristics, but have signaling deficiencies (*38*). For example, in erythroleukemia cells loss of $G\alpha_{16}$ completely blocks calcium signaling by the purinergic receptor $P2Y_2$ (*43*). Overall current studies indicate differing roles for the G_q family members with $G\alpha_q$ playing a more prominent physiological role. Understanding the many interactions of $G\alpha_q$ with respect to receptors, effectors, and regulators will

ultimately shed light onto how $G\alpha_q$ signaling can give a specific cellular response that is both dependent and independent of inositol lipid signaling.

Regulation of $G\alpha_q$ Signaling

Intrinsic GTPase Activity

G protein signaling is terminated upon hydrolysis of GTP to GDP with $G\alpha$ reassociating with $G\beta\gamma$ and forming the inactive heterotrimeric G protein. Our current understanding of the mechanism of GTP hydrolysis has come from a series of crystal structures of the $G\alpha$ subunit bound to GDP (*44, 45*), GDP·P_i (*46, 47*), GTPγS (*48, 49*) and GDP·AlF_4^- (*49, 50*). Aluminum fluoride is a strong activator of $G\alpha$ subunits, and in the GDP·AlF_4^- crystal structure the AlF_4^- ion is in a square planar configuration with the oxygen of the β-phosphate and a water molecule occupying axial positions. Therefore, this ligand mimics the transition-state of GTP hydrolysis. Biochemical and structural studies implicated Arg 178 and Gln 204 ($G\alpha_i$, Figure 3B) as the catalytic residues of GTP hydrolysis. The glutamine residue coordinates and polarizes the catalytic water molecule, and the arginine stabilizes the developing negative charge on the transition state (*11, 17*).

Regulators of G protein Signaling (RGS) Proteins

Initially it was thought that the GTP hydrolysis was an unregulated function of the $G\alpha$ subunits (*51*). However, in the visual cycle the physiological half-lives (~100 ms) were much faster than the *in vitro* half-lives for GTP hydrolysis (~15 s).

Soon after it was discovered that GTPase activating proteins (GAPs) accelerate the catalytic rate of GTP hydrolysis (*12*). The first discovered GAP for Gα subunits was the $G\alpha_q$ effector PLCβ, which could accelerate GTP hydrolysis by more than 50-fold (*52*). More recently, another class of was discovered: the regulator of G protein signaling (RGS) proteins (*53-55*).

RGS proteins can be classified into four families based on sequence homology: R4, R7, R12, and RZ, with R4 being the largest family with nine members (*56*). All RGS proteins share a conserved ~120 amino acid RGS homology (RH) domain that accelerates GTP hydrolysis. While some RGS proteins contain little more than the RH domain (as is common in the R4 family), others have additional domains that are able to regulate RGS activity (*57*).

There are now over seven crystal structures of Gα subunits in complex with RGS proteins (*58*). In each of these structures, the Gα subunit is activated by the non-natural substrate $GDP{\cdot}AlF_4^-$, and the RGS proteins do not donate any catalytic residues to the active site, unlike the Ras GAPs, which contribute an “arginine finger” to promote hydrolysis. Instead, the available evidence indicates that RGS proteins accelerate GTP hydrolysis by stabilizing the transition state of GTP hydrolysis (*16, 59*).

Structurally, there are two important interactions formed between RGS proteins and Gα subunits. Using RGS4-$G\alpha_{i1}$ as an example (Figure 3), the residue $G\alpha_{i1}$-

Thr182 in switch I rotates 120° to make contacts with RGS4-Asn88, allowing for the formation of a hydrogen bond network involving Thr182 and the switch II residues Glu207 and Lys210, which does not occur in the absence of RGS protein. The second key interaction is formed by RGS4-Asn128, which packs against both switch I and II, directing the catalytic glutamine (Gln204) to coordinate the catalytic water and γ-phosphate during the transition state (*11, 16, 58*). Mutation of this residue or its equivalents in other RGS proteins can greatly inhibit GAP activity, as in RGS4-N128A (*60*) and RGS2-N149D (*61*).

In general, the structural differences between the different Gα-RGS interfaces are subtle. However, several RGS proteins exhibit selectivity towards different Gα subunits. For example, RGS4 can serve as a GAP for both $G\alpha_i$ and $G\alpha_q$ (*62*), but RGS2 has been shown to be selective towards $G\alpha_q$ (*63, 64*). Selectivity between the major Gα classes is likely mediated by differences in the RH domain-switch I/II interface, whereas differences in the RH domain-switch III interface could play a role in selectivity among Gα family members (*58*). It is interesting to speculate if effector binding could modify RGS selectivity towards other Gα's.

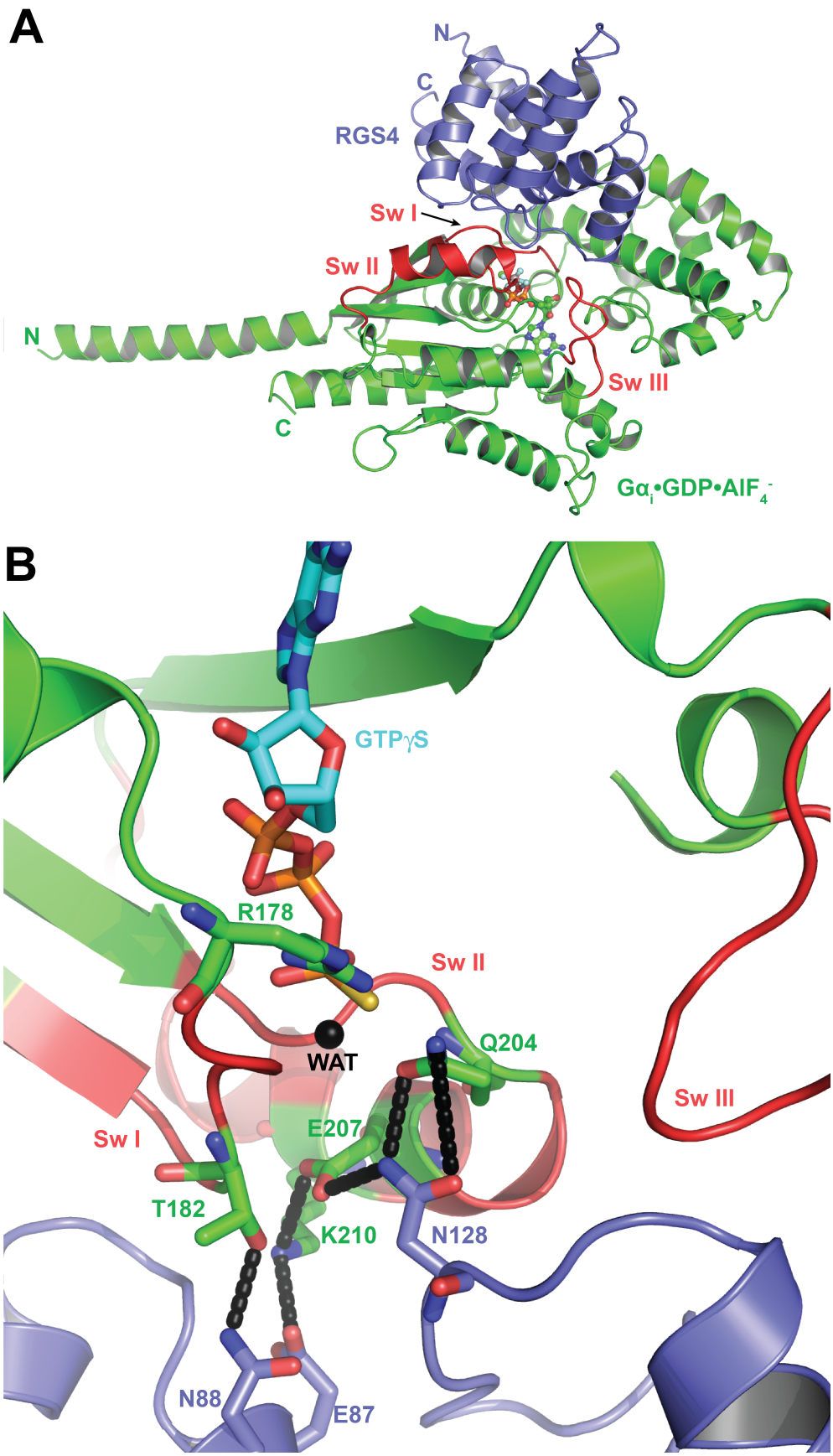
A
N
C
RGS4
Sw I
Sw II
N
Sw III
C
Gαi•GDP•AlF4-
B
GTPγS
R178
Sw II
Q204
WAT
Sw III
Sw I
E207
T182
K210
N128
N88
E87

Figure 3: RGS4 binds to the three switch regions of $G\alpha_i$. A) Structure of $G\alpha_{i1}\cdot GDP\cdot ALF_4^-$ in complex with RGS4. $G\alpha_i$ is colored green and RGS4 is colored blue. The switch regions of $G\alpha_i$ are colored red. RGS4 makes contacts with all three switch regions of $G\alpha_i$ stabilizing the transition state of GTP hydrolysis. **B)** A close-up view of the $G\alpha_i$-RGS4 interface with GTPγS modeled from the $G\alpha_i\cdot GTP\gamma S$ structure (PDB:1GIA) in place of $GDP\cdot AlF_4^-$. RGS4 does not directly take part in the catalysis of GTP hydrolysis.

G protein-coupled Receptor Kinase 2 (GRK2)

G protein-coupled receptor kinases (GRKs) are members of the protein kinase A (PKA), G, and C (AGC) family of kinases that phosphorylate serine/threonine residues on the third cytoplasmic loop or carboxyl terminal tail of agonist bound GPCRs (*65*). Receptor phosphorylation promotes the binding of arrestin, which uncouples receptors from G proteins and targets them for endocytosis (*13, 15*). There are seven mammalian GRKs that are classified into three subfamilies based on their gene structure and homology: GRK1 (GRK1 and -7), GRK2 (GRK2 and -3), and GRK4 (GRK4-6). All GRKs have a similar overall structure with a N-terminal RH domain, a central catalytic kinase domain, and a less conserved C terminal domain that is typically involved in targeting the kinases to the plasma membrane. For example, the GRK2 family contains a pleckstrin homology (PH) domain in the C-terminus that binds free $G\beta\gamma$ subunits, resulting in recruitment to the plasma membrane (*66*).

In addition to inhibiting GPCR function via phosphorylation, GRK2 has been shown to inhibit signaling via a phosphorylation independent mechanism on numerous $G\alpha_q$-coupled receptors including: the angiotension II receptor (*67*), the endothelin A and B receptors (*68*), the thromboxane A2 receptor (*29*), the parathyroid hormone receptor (PTH) (*69*), the M_1 muscarinic acetylcholine receptor (M_1AChR) (*70*), and the metabotropic glutamate 1a receptor (*71*). The mechanism of the phosphorylation independent densensitization was attributed to the N-terminal RH domain of GRK2, both biochemically and structurally (*25, 26, 29*). Initial studies showed that activated $G\alpha_q$ could bind GRK2 (and GRK3), and that overexpression on the N-terminal RH domain was sufficient to attenuate signaling through $G\alpha_q$. Furthermore, a kinase deficient mutant of GRK2 (K220R) was capable of desensitizing $G\alpha_q$-coupled receptors (*72*).

Although one might initially expect GRK2 to regulate $G\alpha_q$ activity by acting as a GAP, given its RH domain, GRK2 has little or no GAP activity (*29, 73*). Additionally, mutagenesis studies showed that GRK2 has two unique residues (Arg106 and Asp110) that are required for $G\alpha_q$ binding, which are not in equivalent positions used by RGS proteins to bind $G\alpha$ subunits (*74, 75*). The crystal structure of the $G\alpha_q$-GRK2-$G\beta\gamma$ complex (Figure 4C) (*26*) revealed that GRK2 binds $G\alpha_q$ much like an effector, as seen in the structures of $G\alpha_s$-AC (Figure 4A) (*76*), $G\alpha_t$-PDEγ-RGS9 (*77*), $G\alpha_{13}$-p115RhoGEF (*78*), and the more

recently solved structure of the $G\alpha_q$-p63RhoGEF-RhoA complex (Figure 4B) (*24*).

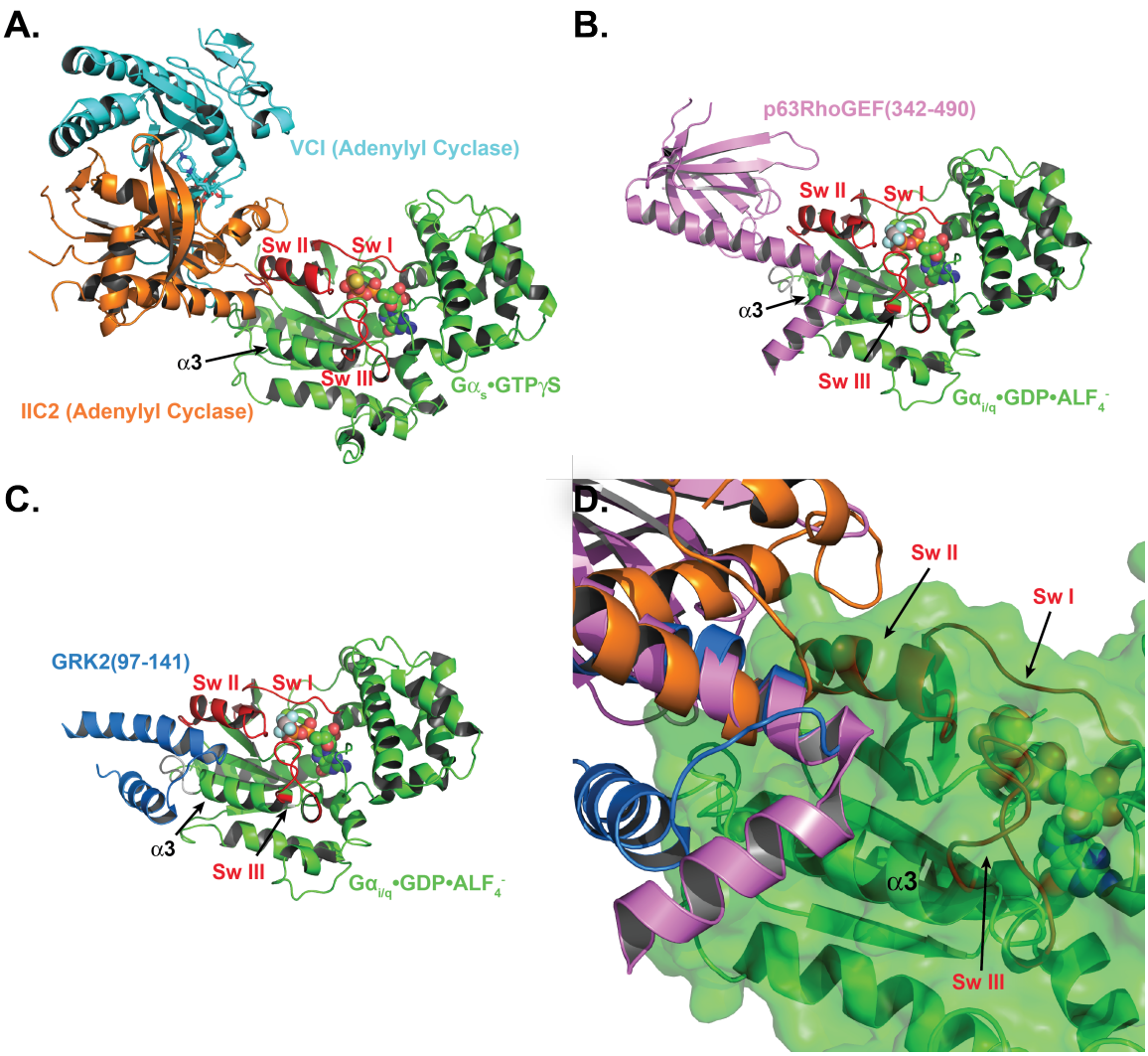

Figure 4: Gα-effector complexes. All Gα subunits are colored in green with the switch regions in red. **A)** $G\alpha_s$·GTPγS in complex with the VC_1 and IIC_2 subunits of adenylyl cyclase, respectively colored cyan and orange (PDB: 1CJT). **B)** $G\alpha_{i/q}$·GDP·AlF_4^- in complex with residues 343-490 of p63RhoGEF colored in violet (PDB: 2RGN). **C)** $G\alpha_{i/q}$·GDP·AlF_4^- in complex with residues 97-141 of

GRK2 colored blue (PDB: 2BCJ). **D)** A close-up view of panels (A-C) overlaid onto the surface of $G\alpha_s$·GTPγS (colored in green). Adenylyl cyclase, p63RhoGEF, and GRK2 make extensive contacts with the switch II and α3 helices of Gα subunits.

Evidence for High Order $G\alpha_q$ Signaling Complexes

An important question in cellular signaling is what determines the specificity of the signal transduction process. The collision-coupling model (*79*) suggests that the signaling specificity is solely determined by the structure of the receptor-G protein interaction and the G protein-effector interface. Additionally, the model depicts the individual membrane proteins as being freely dissolved, thus, activated proteins will freely diffuse throughout the membrane until they randomly collide with their target.

A major inconsistency in the collision-coupling model is how do activated proteins, such as G$\beta\gamma$, maintain their signaling specificity within a cell. For example, in cardiomyocytes activation of the β_2-adrenergic receptor (β_2AR) causes $G\alpha_s$-mediated activation of AC. However, in the same cells, the inwardly rectifying potassium channel (Kir 3) is opened by G$\beta\gamma$ in response to activation of $G\alpha_i$ by the M_2-muscuranic receptor (*80*). Thus, according to the collision-coupling model free G$\beta\gamma$ from the activation of β_2AR would also be able to open Kir 3 channels, which does not normally happen in cells, indicating that specificity

is controlled. In this case, specificity could be controlled by pre-formed complexes between receptor, G protein, and effector, preventing cross-talk into another pathway (*81*). Signaling complexes can also combine multiple activities allowing for more efficient control of steady state levels of signaling. Kinetic data shows that $G\alpha_q$, PLCβ1, and the M_1AChR can exist in an activated complex where the GEF activity of the receptor and the GAP activity of PLCβ1 can achieve any physiological rate of activity, without the need of other regulatory proteins (*82*). There is further evidence that RGS proteins can play a role in this complex by acting as a "kinetic-scaffold" that limits the range of G protein signals (*83*).

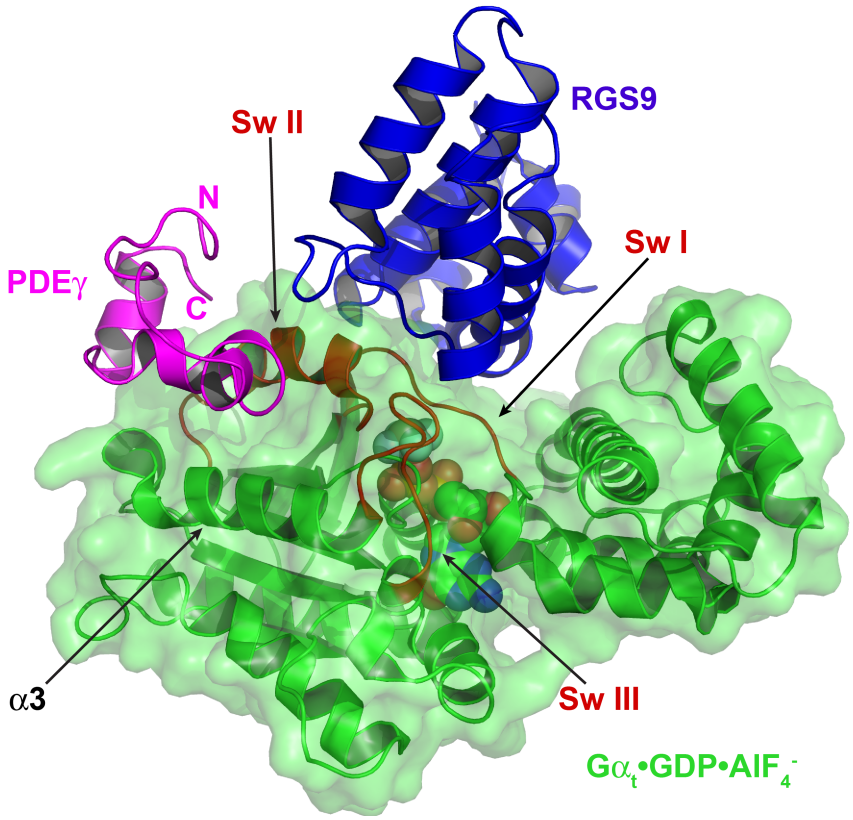

Figure 5: Model of a high order complex with a Gα subunit, effector, and RGS protein. $G\alpha_{t/i}$·GDP·AlF_4^- (green) in complex with PDEγ (magenta) and

RGS9 (blue) (PDB: 1FQJ). Formation of the ternary complex is required to achieve physiological rates of GTP hydrolysis on $G\alpha_t$.

Additional evidence exists for high order signaling complexes given the crystal structures of the $G\alpha_i$-RGS4 (*59*) and $G\alpha_s$-adenylyl cyclase (*76*) complexes, which revealed that RGS proteins and effectors interact with discrete footprints on the surface of $G\alpha$ and have the potential to bind simultaneously, although $G\alpha_s$ is not known to be regulated by RGS proteins. Direct experimental support for an RGS-$G\alpha$-effector ternary complex came from analysis of the interactions of transducin ($G\alpha_t$) with RGS proteins and the γ subunit of cGMP phosphodiesterase (PDEγ). Both PDEγ (*52*) and RGS9 (*84*) are required for physiological rates of GTP hydrolysis on $G\alpha_t$. Although PDEγ has no GAP activity on its own, it can stimulate RGS9-mediated GAP activity by up to ~3 fold (*84*). Mutagenesis studies (*85*), biophysical measurements (*86*), and ultimately the crystal structure of the RGS9-$G\alpha_{t/i1}$-PDEγ ternary complex (Figure 5) (*77*) were all consistent with a model of allosteric modulation between the effector and RGS-binding sites of $G\alpha_t$, with little or no direct functional interaction between PDEγ and RGS9. It has been proposed that this PDEγ-regulated GAP activity prevents a “short-circuit” of the phototransduction cascade via premature hydrolysis of $G\alpha_t$·GTP before effectors can functionally interact with the G protein (*87*). Conversely, PDEγ inhibits the GAP activity of other RGS proteins (RGS4, GAIP and RGS16/RGSr), most likely through a negative allosteric mechanism (*87-89*), supporting the conclusion that RGS9 and $G\alpha_t$ represent a physiologically

relevant pair. It is not known whether similar ternary complexes are formed by other members of the $G\alpha_i$ family or by subunits from the $G\alpha_q$ family, or if there are other effector/RGS combinations that are synergistic with respect to GAP activity on $G\alpha$.

Chapter 2
Assembly of High Order $G\alpha_q$-Effector Signaling Complexes with RGS Proteins

BACKGROUND AND RESEARCH PLAN

The crystal structure of the $G\alpha_q$-GRK2-$G\beta\gamma$ complex revealed that GRK2 binds to the effector-binding site of $G\alpha_q$ (*26*), raising the interesting possibility that GRK2 is in fact an effector that can initiate its own signaling cascades in response to the activation of $G\alpha_q$. Although one obvious pathway is simply the phosphorylation of activated GPCRs, GRK2 has also recently been shown to phosphorylate insulin receptor substrate-1 (IRS-1) (*90*), p38 MAP kinase (*91*), and ezrin (*92*) in response to GPCR activation. Additionally, the binding of GRK2 to $G\alpha_q$ is such that it leaves the RGS binding site accessible. This leads to the question of whether or not GRK2 and RGS proteins can form ternary complexes with $G\alpha_q$.

The rate of GTP hydrolysis by $G\alpha_q$ can be accelerated by many different RGS proteins (*19*), but two of the best characterized are RGS2 and RGS4, which are both members of the RGS B/R4 subfamily (*93, 94*). Both proteins have been reported to serve as effector antagonists because they can inhibit PLCβ signaling by either GTPase-deficient Gα subunits or Gα subunits loaded with non-hydrolyzable GTP analogs (*64, 95, 96*).

In this project, we have used biophysical and kinetic studies to demonstrate the formation of ternary complexes of between $G\alpha_q$, RGS2/4 and the effectors GRK2/p63RhoGEF. We also showed that RGS2 and RGS4 are negative allosteric modulators of proteins that bind to the effector-binding site of $G\alpha_q$, providing a probable molecular basis for their roles as effector antagonists. Conversely, GRK2 and p63RhoGEF are shown to be allosteric modulators of RGS GAP activity. Interestingly, GRK2 stimulates RGS4 GAP activity on $G\alpha_q$ to an extent that is similar to that of PDEγ on RGS9-$G\alpha_t$. These data provide novel insights into the possible mechanisms of regulation of GRK2 and p63RhoGEF by both $G\alpha_q$ and RGS proteins *in vivo*.

METHODS

Purification of RGS2 and RGS4.

Human RGS2 (1-211), ΔN-RGS2(72-211), RGS2(1-72), and RGS2-N149D were cloned into the pMALc2H_{10}T vector using the BamHI and SalI restriction sites and expressed as as a maltose-binding protein (MBP) fusion protein in Rosetta (DE3) pLys cells (*97*). Bacterial cells were grown to an OD_{600} of 0.8 and expression of RGS2 was inducted by the addition of 100ug/mL of isopropylthiogalactopyranoside (IPTG) at 20° C. The cells were harvested after 20 hours by centrifugation and frozen in liquid nitrogen. Cell pellets were resuspended in lysis buffer (20 mM HEPES pH 8.0, 500 mM NaCl, 10 mM β-mercaptoethanol) plus 1 μM leupeptin, 1 mM lima bean trypsin inhibitor and 0.1

mM phenylmethylsulphonyl fluoride. Cells were lysed with an Avestin C3 homogenizer and ultracentrifuged at 40,000 rpm for 1 hr using a Beckman Type Ti 45 rotor. The supernatant was filtered through a glass filter, and then loaded on a Ni-NTA column pre-equilibrated with lysis buffer. The column was washed with 10 column volumes of lysis buffer, followed by 10 column volumes of lysis buffer plus 20 mM imidazole pH=8.0. MBP-RGS2 was eluted with lysis buffer containing 150 mM imidazole pH 8.0, and then treated with 2% (w/w) TEV protease and dialyzed against lysis buffer overnight. The dialysate was passed back over a Ni-NTA column equilibrated with lysis buffer to remove His-tagged MBP and uncut fusion protein. RGS2 was then concentrated in a 30 kDa Centriprep (Millipore) and further purified using two tandem Superdex S200 columns equilibrated with 20 mM HEPES pH 8.0, 500 mM NaCl and 5 mM DTT. All purification steps were performed at 4 ˚C. The yield of pure RGS2 was typically ~5 mgs per liter of culture, and ΔN-RGS2 was ~3 mgs per liter. MBP-RGS2(1-71) is not TEV cleaved and is purified to a final yield of ~1.5 mgs per liter. Due to occasional purification problems associated with RGS2 precipitation, we also produced RGS2 from a $(His)_{10}$-RGS2 pET19B vector (ampicillin resistant, a gift from Scott Heximer, U. of Toronto). Purification of $(His)_{10}$-RGS2 was as previously described (*98*). Rat RGS4 was purified as previously described, as was ΔN-RGS4(51-205), and the RGS4-N128G mutant (a gift from Elliot Ross, UT Southwestern)

Purification of Other Proteins

A $G\alpha_{i/q}$ chimera, in which the amino terminal helix of $G\alpha_q$ is replaced with that of $G\alpha_i$ (*26*), a fragment of human p63RhoGEF spanning residues 149-502 (henceforth referred to as p63RhoGEF), and GRK2 were purified as previously described (*24, 99, 100*). Point mutants GRK2-D110A and p63RhoGEF-F471E were purified as described for their respective wild type proteins.

Flow Cytometry Protein Interaction Assay

Equilibrium binding of either RGS2, RGS4, GRK2, or p63RhoGEF to $G\alpha_{i/q}$ was measured by a flow cytometry protein interaction assay (FCPIA). RGS2 and GRK2 were fluorescently labeled with either an amine reactive probe (Alexa Fluor 532 carboxylic acid, succinimidyl ester) or a thiol reactive probe (Alexa Fluor 532 C_5-maleimide). Both probes gave similar results in binding assays. RGS4 and p63RhoGEF were labeled only with the thiol reactive probe, as amine react probes did not produce sufficient signal. $G\alpha_{i/q}$ was biotinylated using biotinamidohexanoic acid *N*-hydroxysuccinimide ester (Sigma) initially in the form of a $G\alpha_{i/q}\beta\gamma$ heterotrimer, as previously described (*24*). Subsequently, $G\alpha_{i/q}$ was biotinylated directly as a monomer because it behaved similarly and had the advantage of not requiring separation from $G\beta\gamma$. Biotinylated $G\alpha_{i/q}$ (b-$G\alpha_{i/q}$, 5 nM) was linked to *x*Map LumAvidin microspheres (Luminex) and washed three times with 20 mM HEPES pH 8.0, 100 mM NaCl, 5 mM $MgCl_2$, 0.1% lubrol, 2 mM DTT, 1% BSA, 50 μM GDP plus other additions as indicated). The indicated concentrations of Alexa Fluor 532 (AF)-labeled protein were then added to bead-bound b-$G\alpha_{i/q}$ and then allowed to equilibrate for at least 30 min before being

processed on a Luminex 96-well plate bead analyzer. For competition studies, unlabeled proteins were also added as indicated. Longer incubation times (*e.g.* overnight) did not alter the results indicating that equilibrium was attained under our assay conditions. The association of AF-labeled protein with beads is reported as the median fluorescence intensity (MFI) for each sample. Each data point was typically measured in duplicate.

Direct binding and competition data were fit by nonlinear regression either to one-site binding equations or to an allosteric model using GraphPad Prism (v. 5.0a). Allosteric modulation of AF-GRK2 binding to $G\alpha_{i/q}$ by RGS proteins was fit using equations 1 & 2:

$$Y = Y_0 + NS \times [GRK2] + \frac{[GRK2] \times B_{\max}}{[GRK2] + K_d'} \qquad (1)$$

where Y is the total fluorescence measured, Y_0 is the background fluorescence, NS is the linear increase in fluorescence due to non-specific binding of AF-GRK2 to beads, and B_{max} is the maximum fluorescence change due to specific binding. For all but one of the RGS2 dose response curves (Fig. 5B), Y_0 and NS were directly measured and subtracted from the data to obtain specific binding. For these corrected sets, Y_0 and NS were fixed to be 0. K_d' is the apparent dissociation constant for AF-GRK2:

$$K_d' = K_d \times \frac{(K_A + [A])}{(K_A + [A]/\alpha)} \qquad (2)$$

where K_d is the dissociation constant of AF-GRK2 in the absence of allosteric modulation, K_A is the dissociation constant of allosteric modulator A (*i.e.*, RGS2 or RGS4) in the absence of AF-GRK2, and α is the cooperativity factor (*101*). An α value greater than 1 corresponds to negative allostery. K_d, K_A and a were fit globally from 2-5 separate series of binding saturation curves with automatic outlier rejection as implemented by GraphPad Prism. To analyze dose response curves using an alternative competitive model, the [A]/α term was deleted. Model comparisons used the F test as implemented by GraphPad Prism.

Dissociation Rate of GRK2

To determine k_{off} for GRK2 from b-G$\alpha_{i/q}$, 10 nM AF-GRK2 was incubated with bead bound b-G$\alpha_{i/q}$ for 1 or 24 hours at 4° C. Trays were then allowed to equilibrate at room temperature for 30 minutes, and the dissociation of AF-GRK2 was initiated by adding unlabeled GRK2 (final concentration 1 mM), GRK2 plus RGS2 (both 1 μM final), or GRK2 plus RGS4 (both 1 μM final). The loss of fluorescence was measured by FCPIA at the indicated time points. Data were fit to a one phase exponential decay.

RESULTS

Crystallographic Models of Gα_q Effector Complexes with RGS Proteins

Crystallographic studies demonstrated that GRK2 and p63RhoGEF both engage Gα_q in a manner that would appear to allow the binding of the RGS domain of

either RGS4 (*99*) or RGS2 (*62*) to $G\alpha_q$ without steric overlap (Figure 6A, B). Models of these RGS-$G\alpha_{i/q}$-effector complexes thus resemble the structure of the PDEγ-$G\alpha_{i/t}$-RGS9 complex (Figure 6C). The positions of the modeled RGS box domains in these complexes are also consistent with the predicted orientation of these complexes at the cell surface, in that the expected membrane binding elements of the RGS proteins are juxtaposed with the phospholipid bilayer. We therefore initiated *in vitro* experiments to confirm the formation of these complexes and to better understand the roles of RGS proteins in modulating the interactions of $G\alpha_q$ with GRK2 and p63RhoGEF.

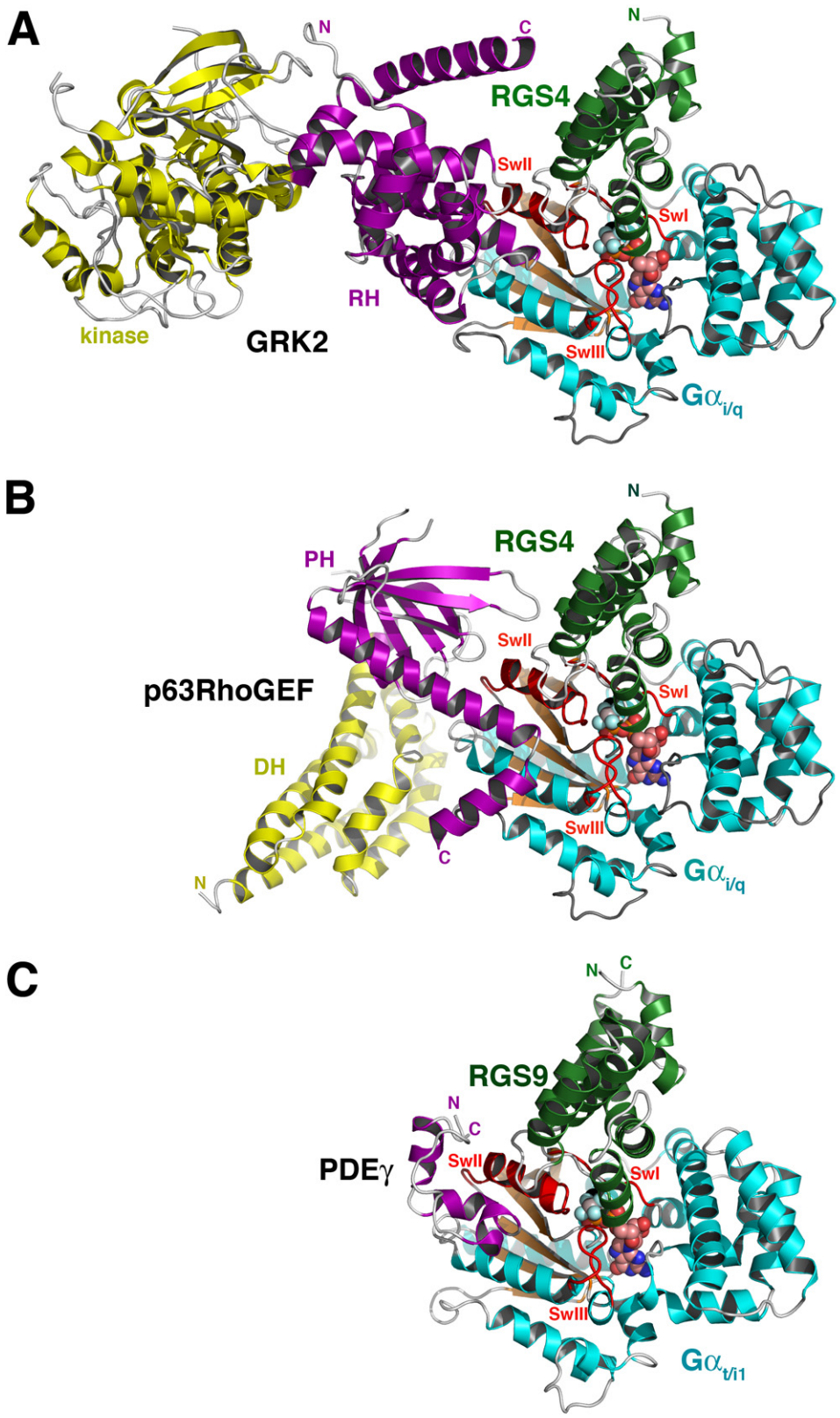
A
N
C
N
RGS4
SwII
SwI
RH
kinase
GRK2
SwIII
Gαi/q
B
N
RGS4
PH
SwII
p63RhoGEF
SwI
DH
SwIII
C
N
Gαi/q
C
N
C
RGS9
N
C
SwII
PDEγ
SwI
SwIII
Gαt/i1

Figure 6: Models of $G\alpha_q$ effector complexes with RGS proteins. Figure by Dr. Aruna Shankaranarayanan. To generate these models, the structure of $G\alpha_{i/q}$ in the $G\alpha_{i/q}$-GRK2-$G\beta\gamma$ complex (PDB ID: 2BCJ) and $G\alpha_{i/q}$ in the $G\alpha_{i/q}$-p63RhoGEF-RhoA complex (PDB ID: 2RGN) were superimposed on $G\alpha_i$ in the $G\alpha_i$-RGS4 structure (PDB ID: 1AGR), which positioned RGS4 at the RGS-binding site on the surface of $G\alpha_{i/q}$. There was no obvious steric overlap between the docked-RGS4 and either GRK2 or p63RhoGEF except for the protruding β6-β7 loop of the p63RhoGEF PH domain, which would come into contact with the α3 helix of the RGS box domain. However, this loop can likely adopt many conformations. Both the $G\alpha_q$-GRK2-$G\beta\gamma$ and $G\alpha_q$-p63RhoGEF peripheral membrane complexes contain markers, including the prenylation sites of $G\gamma$ and RhoA, that help define how the complexes could be oriented with respect to the cell surface. The expected membrane surface is parallel to the top of each panel. **A)** Model of RGS4 bound to the $G\alpha_{i/q}$-GRK2 complex. The PH domain of GRK2 was omitted for clarity. $G\alpha$ is colored cyan with orange β-strands, and the three switch regions (SwI, SwII and SwIII) are colored red. $Mg^{2+}{\cdot}GDP{\cdot}\ AlF_4^-$ in the active site of $G\alpha_{i/q}$ is shown as a sphere model. Carbons are colored rose, nitrogens blue, oxygens red, Mg^{2+} black, Al^{3+} sand, and F^- light blue. The kinase and RGS homology domains of GRK2 are colored yellow and purple, respectively, and RGS4 is green. N and C denote the observed amino and carboxyl termini of the proteins. **B)** Model of RGS4 bound to the $G\alpha_{i/q}$-p63RhoGEF complex. The DH and PH domains of p63RhoGEF are colored yellow and purple, respectively. **C)** Structure of the RGS9-$G\alpha_{t/i1}$-PDEγ

complex (PDB ID: 1FQJ) with the Gα subunit in the same orientation as $G\alpha_{i/q}$ in panels A and B. PDEγ and RGS9 are colored purple and green, respectively.

Direct Binding of Fluorophore Labeled Proteins

To observe formation of ternary RGS complexes in vitro, we chose to use a flow-cytometry protein interaction assay (FCPIA), wherein a protein receptor is biotinylated and bound to streptavidin-coated beads, and the equilibrium binding of a fluorescently-labeled ligand is quantitatively assessed by measuring bead-bound fluorescence in a flow cytometer (*102, 103*). We first measured the direct association of Alexa Fluor 532 (AF)-labeled GRK2 (AF-GRK2), AF-p63RhoGEF, AF-RGS2 and AF-RGS4 with a biotinylated chimera of $G\alpha_q$·GDP (b-$G\alpha_{i/q}$) bound to the streptavidin beads and activated with AlF_4^- (Figure 8A). Non-specific binding was determined from the increase in fluorescence using the deactivated, GDP-bound chimera. We used a $G\alpha_q$ chimera ($G\alpha_{i/q}$), wherein the amino terminal helix of $G\alpha_q$ is substituted with that of $G\alpha_i$, because the protein can be expressed recombinantly at much higher yields in insect cells (*26, 104*). Based on the available crystal structures of the $G\alpha_q$-p63RhoGEF and $G\alpha_q$-GRK2 complexes (Figure 6A,B), the amino terminus of $G\alpha_q$ is not expected to directly interact with these effectors. Furthermore, the binding of GRK2 to a different chimera of $G\alpha_q$ that included the native amino terminus of $G\alpha_q$ yielded similar dissociation constants as with $G\alpha_{i/q}$ (Figure 8). The p63RhoGEF construct used in this study spans residues 149 through 502 of the full length protein and is the

minimal fragment required for high-affinity $G\alpha_{i/q}$ binding and activation *in vitro* and for full $G\alpha_q$-mediated activation of RhoA *in vivo* (*24*). AF-GRK2, AF-p63RhoGEF, AF-RGS2 and AF-RGS4 bound to $G\alpha_{i/q}$ with dissociation constants of 3, 80, 3, and 5 nM, respectively (Table 1, Figure 7B-D). When comparing the binding curves for each of the labeled proteins, it is important to note that they are not expected to saturate at the same median fluorescent intensity (MFI) due to different efficiencies of fluorescent labeling.

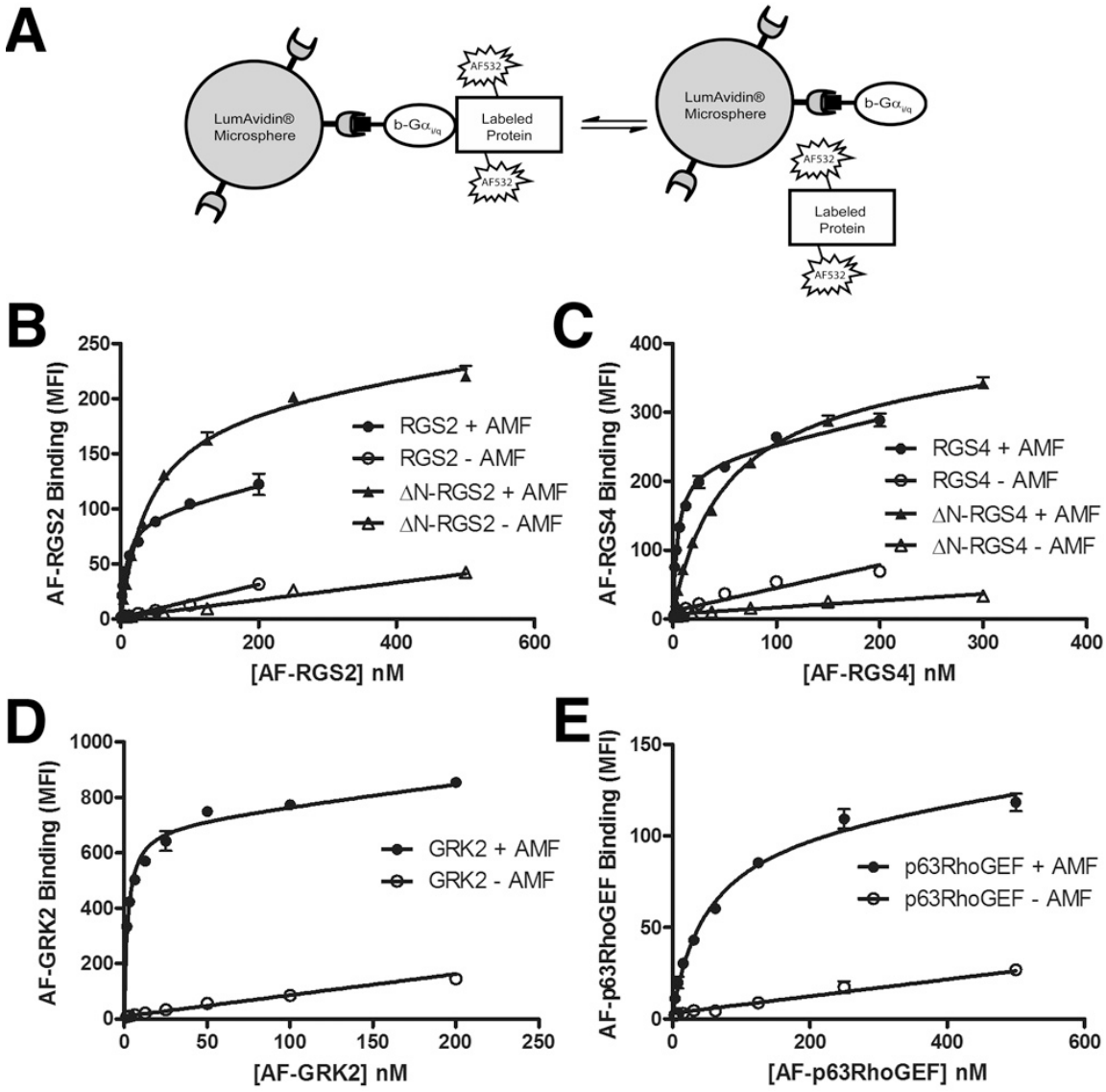

Figure 7: Direct binding of fluor-labeled proteins to $G\alpha_{i/q}$. A) Scheme depicting measurement of equilibrium binding by FCPIA. Total binding was measured on a Luminex flow cytometer as the median fluorescence intensity (MFI) of AF-labeled proteins associated with AlF_4^--activated $G\alpha_{i/q}$ (+AMF) that was biotinylated and bound to streptavidin coated beads. Non-specific binding was measured using bead-bound deactivated $G\alpha_{i/q}$·GDP (-AMF). Total and non-specific binding curves for **B)** RGS2 and ΔN-RGS2, **C)** RGS4 and ΔN-RGS4, **D)**

GRK2, and **E)** p63RhoGEF. The data shown are mean ± SEM values representative of three or more experiments, each run in duplicate.

Table 1: Affinity of effectors and RGS proteins for biotin-G$\alpha_{i/q}$. K_i values were determined with the Cheng-Prusoff equation using the corresponding K_d values for the AF-labeled protein.

	AF-labeled (K_d± S.D.; direct binding)	Unmodified (K_i± S.D.; competition)
RGS2	2.5 ± 1.3 nM	6.4 ± 5.9 nM
ΔN-RGS2	37 ± 12 nM	--
RGS4	5.3 ± 3.0 nM	8.6 ± 4.7 nM
ΔN-RGS4	51 ± 8.3 nM	--
GRK2	3.2 ± 1.7 nM	3.3 ± 1.6 nM
p63RhoGEF	83 ± 34 nM	48 ± 14 nM

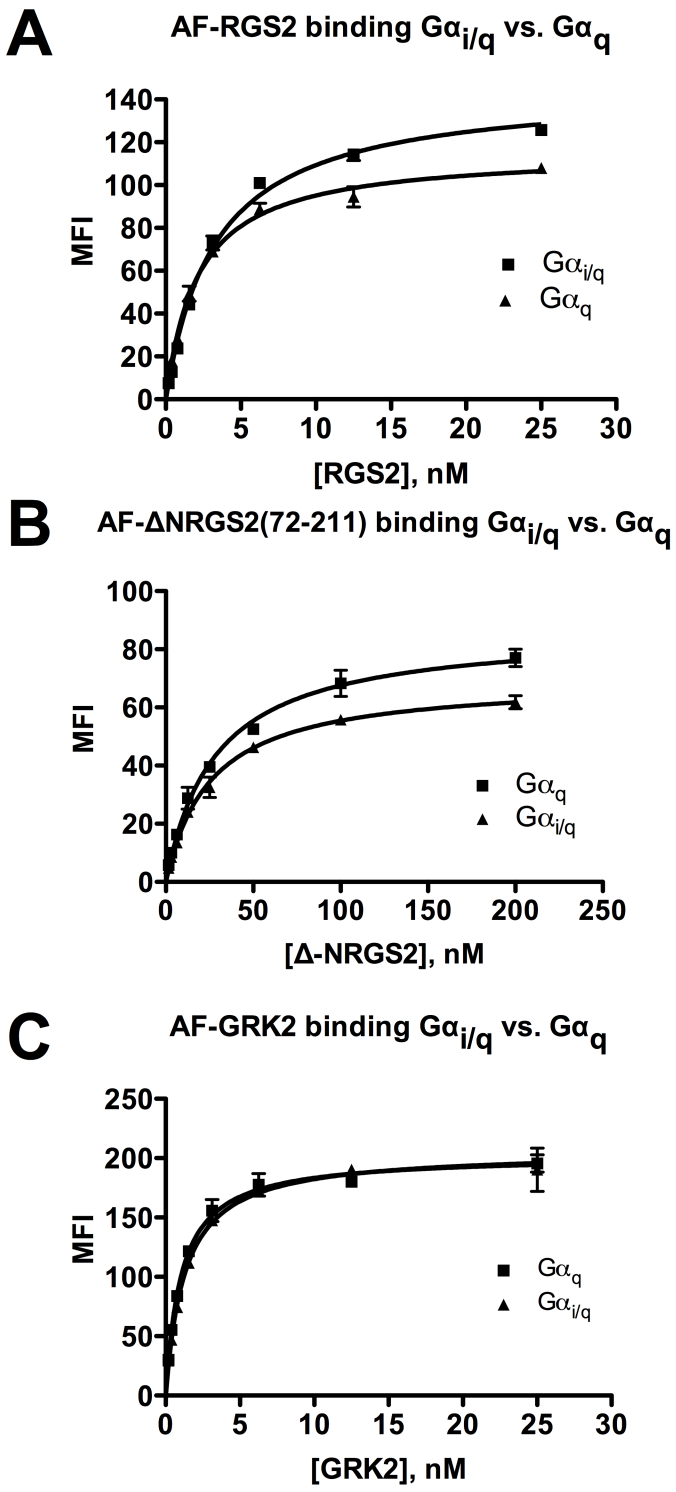
A
AF-RGS2 binding Gαi/q vs. Gαq
MFI
[RGS2], nM
Gαi/q
Gαq
B
AF-ΔNRGS2(72-211) binding Gαi/q vs. Gαq
MFI
[Δ-NRGS2], nM
Gαq
Gαi/q
C
AF-GRK2 binding Gαi/q vs. Gαq
MFI
[GRK2], nM
Gαq
Gαi/q

Figure 8: RGS2 and GRK2 binding to a $G\alpha_q$ variant with a native N-terminus. The $G\alpha_{i/q}$ chimera was used in our binding studies due to the much higher yields of protein from purification. **A)** RGS2, **B)** ΔN-RGS2, and **C)** GRK2 bind to a variant of $G\alpha_q$ that has a native amino terminus. The binding affinities are to that of $G\alpha_{i/q}$ with K_d's of approximately 3.0 nM, 30.0 nM, and 1.0 nM, respectively. The curves have been background subtracted. The data shown is mean ± SEM of duplicate samples from a representative experiment of n≥3 performed.

Competition Assays

Because an AF-labeled protein may not bind with the same affinity as the unmodified protein, we used homologous competition experiments (Figure 9A) to determine the equilibrium dissociation constants for GRK2, p63RhoGEF, RGS2, and RGS4. In these experiments, increasing amounts of unlabeled protein is used to compete against the AF-labeled protein, whose concentration is held at near its measured dissociation constant (Table 1, Figure 8). The resulting IC_{50} values are then converted to K_i values using the Cheng-Prusof equation. K_i values of 3, 50, 6 and 9 nM were measured for GRK2, p63RhoGEF, RGS2 and RGS4 (Table 1, Figure 9B-E, respectively).

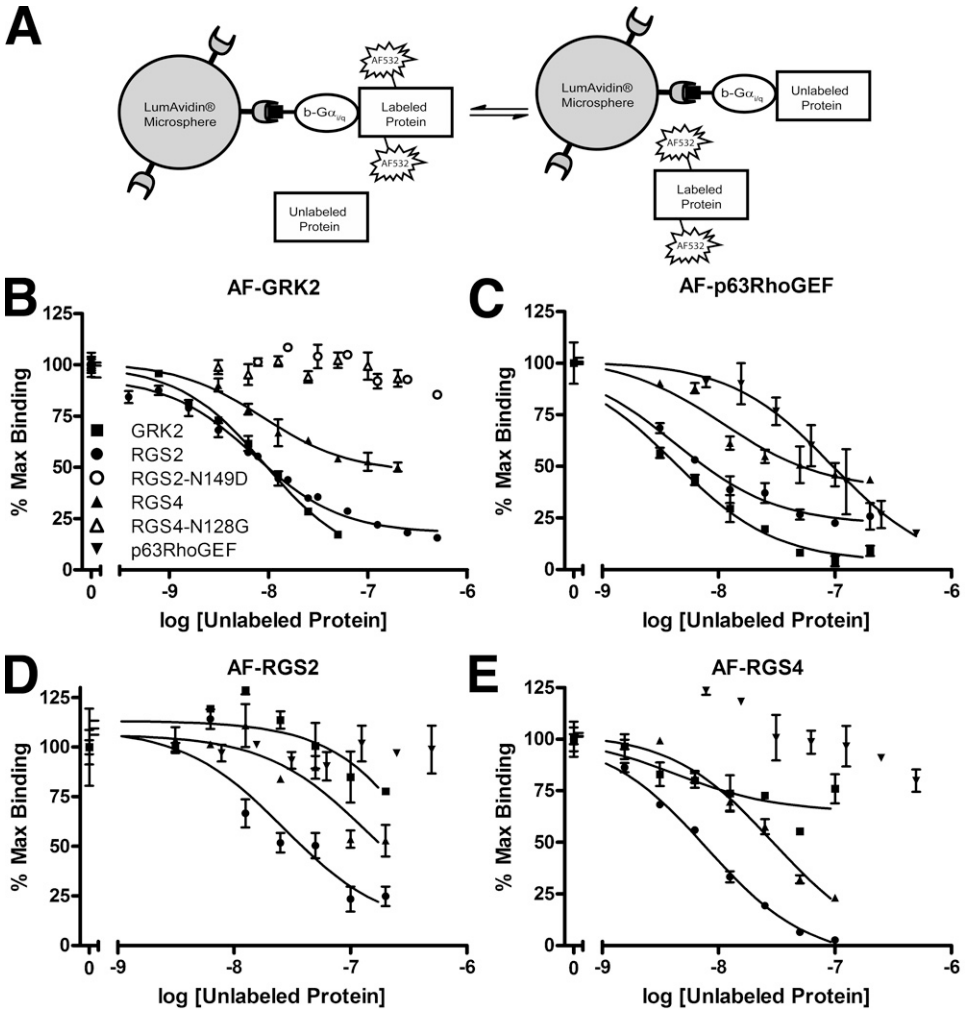

Figure 9: Competition of GRK2 or p63RhoGEF with RGS proteins for b-$G\alpha_{i/q}$. **A)** Scheme depicting FCPIA competition experiments. Increasing amounts of unlabeled protein were mixed with an AF-labeled protein fixed at a concentration near its measured K_d for $G\alpha_{i/q}$. Subsequently, bead-bound b-$G\alpha_{i/q}$·AlF_4^- was added and allowed to equilibrate for at least 30 minutes before measurement. The data was normalized to the uninhibited maximum MFI value for each curve. The data, representative of three or more experiments run in duplicate with mean ± SEM shown, were fit to sigmoidal dose-response curves. **B)** Competition of unlabeled GRK2, RGS2, RGS2-N149D, RGS4, and RGS4-

N128G with 5 nM AF-532 GRK2 for binding to b-$G\alpha_{i/q}$·AlF_4^-. **C-E)** Competition of (C) 50 nM AF-p63RhoGEF, **D)** 10 nM AF-RGS2, and **E)** 10 nM AF-RSG4 with unlabeled p63RhoGEF, GRK2, RGS2, or RGS4 for binding to b-$G\alpha_{i/q}$·AlF_4^-.

We next used FCPIA to examine whether RGS proteins could modulate formation of the $G\alpha_{i/q}$-GRK2 complex. Both RGS2 and RGS4, but not inactive point mutants of RGS2 and RGS4 (N149D (*61*) and N128G (*105*), respectively), could compete with AF-GRK2 binding in the FCPIA assay (Figure 9B). RGS4 could only inhibit AF-GRK2 binding to about 50%, while RGS2 inhibited nearly to completion. Conversely, GRK2 was not an efficacious inhibitor of the binding of either AF-RGS2 (Figure 9D) or AF-RGS4 (Figure 9E) to $G\alpha_{i/q}$ at the concentrations tested. Taken together, these data are most consistent with RGS2 and RGS4 acting as negative allosteric modulators of AF-GRK2 binding to $G\alpha_{i/q}$.

Next, we tested if RGS proteins could modulate formation of the $G\alpha_{i/q}$-p63RhoGEF complex. As a control, we tested if GRK2 acted as an orthosteric inhibitor of AF-p63RhoGEF binding, as would be expected for two proteins that bind at the same site (Figure 6). Indeed, both GRK2 and unlabeled p63RhoGEF fully inhibited binding of AF-p63RhoGEF (Figure 9C). Higher concentrations of p63RhoGEF were required for full competition, consistent with its ~10-fold higher K_d (Table 1). Both RGS2 and RGS4 could compete with AF-p63RhoGEF binding to $G\alpha_{i/q}$ (Figure 9C), but neither could fully inhibit binding. Similar to GRK2,

p63RhoGEF could not efficiently compete against AF-RGS2 and AF-RGS4 binding at the concentrations tested (Figure 9D,E, respectively). The data is thus consistent with RGS2 and RGS4 acting as negative allosteric modulators of p63RhoGEF-$Ga_{i/q}$ complex formation.

Formation of Ternary Complexes by FCPIA

The allosteric behavior observed in the competition experiments represents only indirect proof of the formation of a ternary RGS-$G\alpha_{i/q}$-GRK2/p63RhoGEF complex. To use FCPIA to directly test for the formation of an RGS2/4-$G\alpha_{i/q}$-GRK2 complex, biotinylated RGS proteins (b-RGS2 or b-RGS4) were bound to streptavidin-coated beads, and then incubated in the presence of a fixed concentration of unlabeled $G\alpha_{i/q}$ and increasing amounts of AF-GRK2 or AF-p63RhoGEF (Figure 10A). In this experiment, fluorescence should only be observed when a ternary complex is formed, with $G\alpha_{i/q}$ bridging the bead-bound and AF-labeled proteins. As a control, we first showed that GRK2 has no measurable affinity for RGS proteins, because in the absence of $G\alpha_{i/q}$ the fluorescence signal was similar to that of beads alone (data for RGS4 is shown in Figure 10B). In the presence of $G\alpha_{i/q}\cdot AlF_4^-$, b-RGS4 exhibited saturable binding to AF-GRK2 (Figure 10B,C). The measured K_d for AF-GRK2 binding to RGS4-$G\alpha_{i/q}$ under these conditions was ~4-fold (n=4) higher than its intrinsic dissociation constant for $G\alpha_{i/q}$. This could be a direct result of allosteric modulation of the GRK2-binding site on $G\alpha_{i/q}$ by RGS4. Conversely, RGS2 exhibited no or little ability to form an analogous ternary complex under the

conditions tested (Figure 10C), perhaps consistent with the fact that it exhibits stronger negative allosteric effects than RGS4 (Figure 9C).

Analogous experiments with p63RhoGEF gave similar but less reproducible results, most likely due to the lower maximal signal to noise we routinely observe using AF-p63RhoGEF (cf. Figure 7D & E) and the lower affinity of p63RhoGEF for $G\alpha_{i/q}$ relative to GRK2 (Table 1). However, we could directly confirm the formation of an RGS4-$Ga_{i/q}$-p63RhoGEF complex by size exclusion chromatography (Figure 10D,E). In the experiment shown, a complex of AlF_4^--activated $G\alpha_{i/q}$ with p63RhoGEF was formed, and then excess GDP and Mg^{2+} was removed before addition of apo-RhoA (the presence of GDP and Mg^{2+} inhibits RhoA binding to p63RhoGEF). All four proteins eluted as a single peak from two tandem S200 gel filtration columns (Figure 10D,E). Because $G\alpha_{i/q}$ was limiting, peaks corresponding to free p63RhoGEF, RGS4 and RhoA were observed at lower molecular weights (Figure 10E). Thus, we have both direct (Figure 10) and indirect evidence (Figure 9) that RGS4 has the ability to form ternary complexes with $G\alpha_{i/q}$ and either GRK2 or p63RhoGEF.

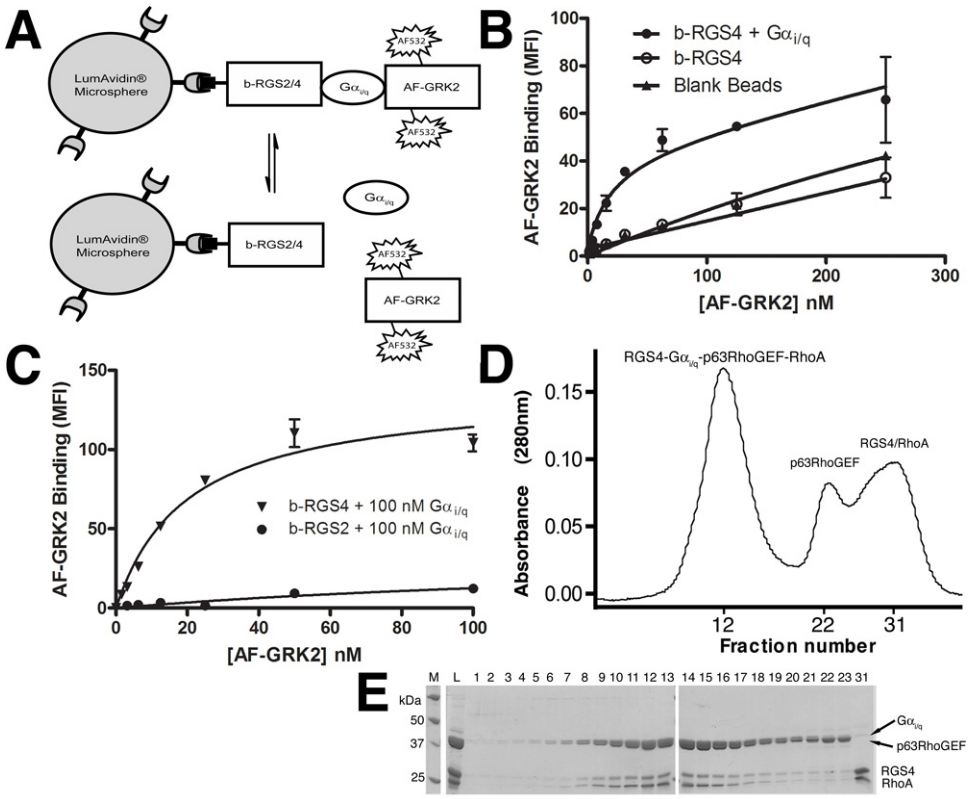

Figure 10: Formation of ternary and higher order RGS complexes with $G\alpha_{i/q}$. **A)** Scheme depicting the direct measurement of ternary complex formation using FCPIA. **B)** AF-GRK2 does not bind to RGS4 in the absence of $G\alpha_{i/q}{\cdot}AlF_4^-$. Shown is the total binding of AF-GRK2 to LumAvidin beads ± b-RGS4 in the presence or absence of activated $G\alpha_{i/q}$. The measured fluorescence of AF-GRK2 binding to beads plus b-RGS4 was similar to that of binding to beads alone. **C)** Specific binding of AF-GRK2 to RGS4-$G\alpha_{i/q}{\cdot}AlF_4^-$. In this experiment, 5 nM b-RGS2 or b-RGS4 was coupled to beads, and then added to AF-GRK2 ± 100 nM $G\alpha_{i/q}{\cdot}AlF_4^-$. RGS2 exhibited little or no affinity under these conditions. Nonspecific binding was measured as the binding of AF-GRK2 to b-RGS2/4 in the absence of $G\alpha_{i/q}$. Data shown is mean ± SEM typical of 4 experiments, each run in duplicate. **D)** Isolation of an RGS4-$G\alpha_{i/q}$–p63RhoGEF-

RhoA quaternary complex by size exclusion chromatography. Ternary complexes of RGS4-$G\alpha_{i/q}$–p63RhoGEF can also be purified (data not shown). **(E)** Peak fractions of the size exclusion run analyzed by SDS-PAGE. Proteins were visualized by Coomassie blue stain. 'M' denotes the protein standard marker lane and 'L' the reaction mix load. (Experiments in panels **D** and **E** were performed by Dr. Aruna Shankaranarayanan)

Role of the N-terminus of RGS2 and RGS4

We had thus far only observed direct ternary complexes with RGS4 in our FCPIA pull-down assay and size exclusion experiments (Figure 10). Although one might expect RGS2 and RGS4 to function similarly, in the absence of any RGS2-Gα crystal structures, it remained possible that RGS2 interacts with $G\alpha_{i/q}$ in a way that overlaps with the effector binding site. The N149D mutant of RGS2, equivalent to N131D point mutant in RGS16 (*61*) and analogous to the N128G mutant of RGS4 (*105*), alters a key residue that packs in the interface between RGS proteins and Gα subunits (*99*). As described earlier, neither RGS2-N149D nor RGS4-N128G could compete against AF-GRK2 for binding $G\alpha_{i/q}$ (Figure 9B). Thus, the RGS box domains of RGS2 and RGS4 likely interact in the same way with the switch regions of the Gα subunit (Figure 6). However, the amino terminal regions of these RGS proteins, which are not typically ordered in crystal structures, also have the potential to influence their behavior. In the R4 family of RGS proteins, an amphipathic helix in the amino terminus is postulated to direct targeting of the RGS protein to membranes (*103, 106-108*) or to the intracellular

loops of GPCRs (*109*), or to inhibit adenylyl cyclase (*110*) and the Ca^{2+} channel TRPV6 (*111*). In our direct binding experiments, deletion of the amino termini of RGS2 (ΔN-RGS2) and RGS4 (ΔN-RGS4) decreased affinity for $G\alpha_{i/q}$ 15- and 10-fold, respectively, compared to the full-length proteins (Figure 7B-C, Table 1). Thus, the amino termini of RGS2 and RGS4 either directly or indirectly contribute to binding affinity for $G\alpha_{i/q}$. To test the possibility that the amino terminus of RGS2, but not RGS4, docks with the effector-binding site of $G\alpha_q$ and thereby inhibits effector binding, we examined the binding of RGS2 and RGS4 to a panel of $G\alpha_q$ mutants known to be defective in effector binding (A253K, T257E, Y261N, and W263D) (*112*) and (A. Shankaranarayanan, unpublished data). In a bead pull-down assay, all of these mutants appeared to bind RGS2 and RGS4 equally well (data not shown). Thus, we have no evidence that RGS2 and RGS4 bind in a fundamentally different way to $G\alpha_q$. It is possible that the amino termini of RGS2 and RGS4 contribute to binding in conjunction with the RGS box through non-specific interactions (note higher non-specific binding for full length RGS2 and RGS4 in Figure 7B-C).

Allosteric Modulation between the RGS and Effector Binding-Sites

To more rigorously examine the allostery mediated by RGS2 and RGS4 on $G\alpha_{i/q}$ complex formation, we used FCPIA to measure the binding of AF-GRK2 to b-$G\alpha_{i/q}{\cdot}AlF_4^-$ in the presence of increasing concentrations of either RGS2 or RGS4 (Figure 11A,B). As expected for negative allosteric modulators (*101*), increasing amounts of RGS2 and RGS4 induced increases in the apparent K_d of AF-GRK2

that saturated at high concentrations of RGS protein. RGS2 (Figure 11A) was more potent than RGS4 (Figure 11B). The data were globally fit to either a simple allosteric ternary complex model (Figure 11,B) or a direct competition model (Figure 12). The curves were best fit by the allosteric model (*101*) with F statistics of 61 and 43 for RGS2 and RGS4, respectively, both with p values < 0.0001. The cooperativity factor (α) for RGS2 was estimated to be 22 ± 2.3 (5 separate series of curves) and that of RGS4 to be 5 ± 0.5 (2 separate series of curves). Thus, RGS2 and RGS4 appear to lower the apparent affinity of GRK2 for $G\alpha_{i/q}$ by up to ~22- and 5-fold, respectively. These allosteric constants were also consistent with the relative extents by which RGS2 and RGS4 inhibited binding of AF-GRK2 in competition curves (Figure 9B). The extracted dissociation constants of GRK2 from the global fits were 3 ± 0.2 and 5 ± 0.5 nM for the RGS2 and RGS4 curves, respectively. The estimated dissociation constants for RGS2 and RGS4 were 10 ± 1 and 80 ± 20 nM, respectively. The GRK2 and RGS2 K_d values are similar to the dissociation constants measured by competition (Table 1) and confirm the validity of the fit to the RGS2 dose response curves. The 10-fold higher K_d calculated for RGS4 is likely a consequence of the smaller allosteric effect of RGS4 and hence greater inaccuracy in the global fit. Analogous experiments for AF-p63RhoGEF binding were not attempted because of its intrinsically lower signal-to-noise ratio in FCPIA measurements (Figure 7).

Another definitive characteristic of an allosteric modulator is to change the rate of dissociation of an orthosteric ligand (*113*). We therefore used FCPIA to measure the dissociation rate of AF-GRK2 from $G\alpha_{i/q}$ in the presence of saturating amounts of unlabeled GRK2, GRK2+RGS2 or GRK2+RGS4 (Figure 11C). RGS2 enhanced the dissociation rate of GRK2 from 0.05 to 0.17 min^{-1}, or 3.3 fold, ANOVA $p<0.0001$. The slight increase in the dissociation rate of GRK2 in the presence of RGS4 (0.065 min^{-1}) was not statistically significant. A 3.3-fold increase in the rate of dissociation is not enough to account for the 22-fold decrease in affinity of GRK2 for $G\alpha_{i/q}$ mediated by RGS2 (Figure 11A). Thus, RGS2 must also decrease the rate of association of GRK2 with $G\alpha_{i/q}$ by ~6 fold. The significant increase in k_{off} mediated by RGS2 (Figure 11C), the superior fits of our data to an allosteric model (Figure 11A,B, Figure 12), and the allosteric behavior exhibited by our competition experiments (Figure 8) all strongly suggest that RGS2 and RGS4 are strong and weak allosteric modulators, respectively, of the effector-binding site of $G\alpha_q$. The fact that RGS2 ternary complexes have thus far proved more difficult to demonstrate directly may simply reflect this stronger allosteric modulation and the correspondingly greater rates that proteins dissociate from RGS2 ternary complexes.

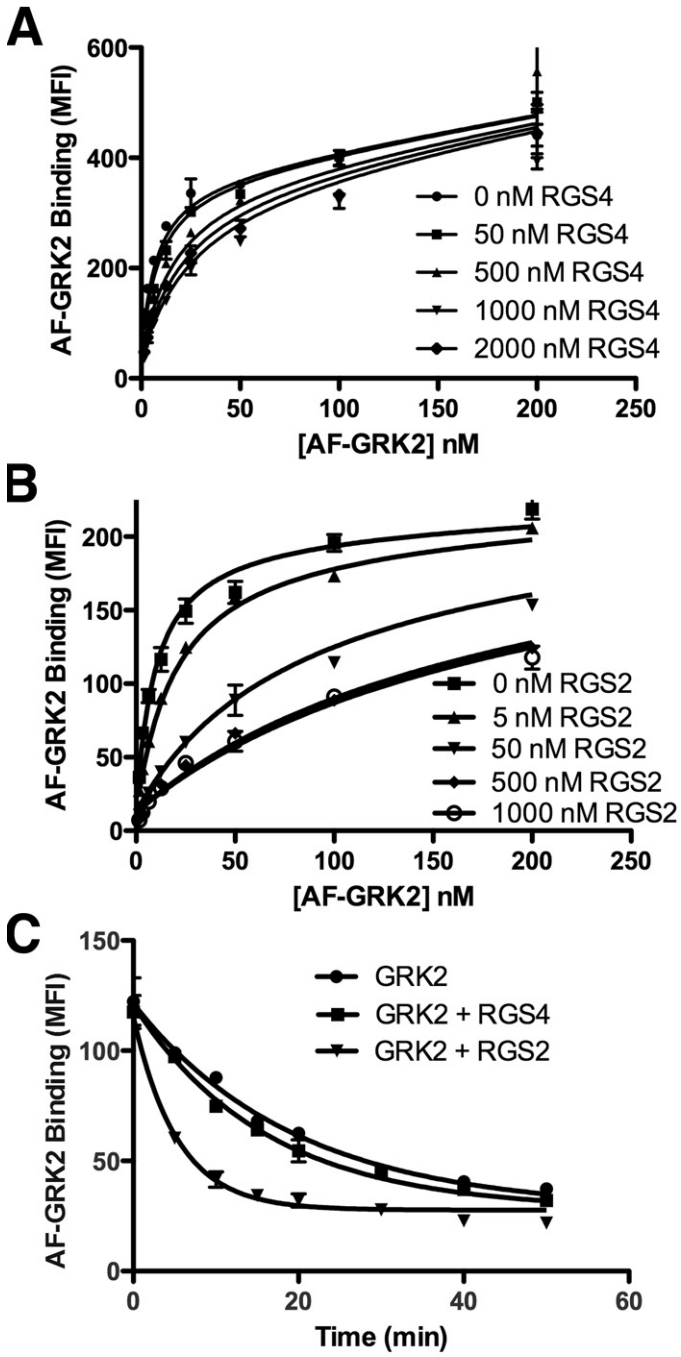

Figure 11: Negative allosteric modulation between RGS proteins and GRK2 for G$\alpha_{i/q}$ binding. A-B) Dose-response curves of AF-GRK2 binding to b-G$\alpha_{i/q}$ in the presence of increasing concentrations of either A) RGS4 or B) RGS2. A model of negative allosteric modulation best fit the data, in part because

increasing concentrations of RGS protein eventually saturate in their ability to increase the apparent K_d of AF-GRK2. The data shown is typical of 2 (RGS4) or 5 (RGS2) sets of experiments, wherein each individual curve was measured in duplicate. **C)** RGS2 modulates the intrinsic rate of GRK2 dissociation from $G\alpha_{i/q}$. The dissociation rate of AF-GRK2 (10 nM) from bead-bound b-$G\alpha_{i/q}\cdot AlF_4^-$ was measured in the presence of either 1 μM GRK2, 1 μM GRK2 plus 1 μM RGS2, or 1 μM GRK2 plus 1 μM RGS4 using FCPIA. The data shown is mean ± SEM representative of one of three experiments, each run with duplicate samples. RGS2 increased k_{off} of GRK2 from 0.054 ± 0.003 min^{-1} to 0.16 ± 0.039 min^{-1} (ANOVA $p<0.01$). RGS4 had a much smaller effect (0.069 ± 0.014 min^{-1}).

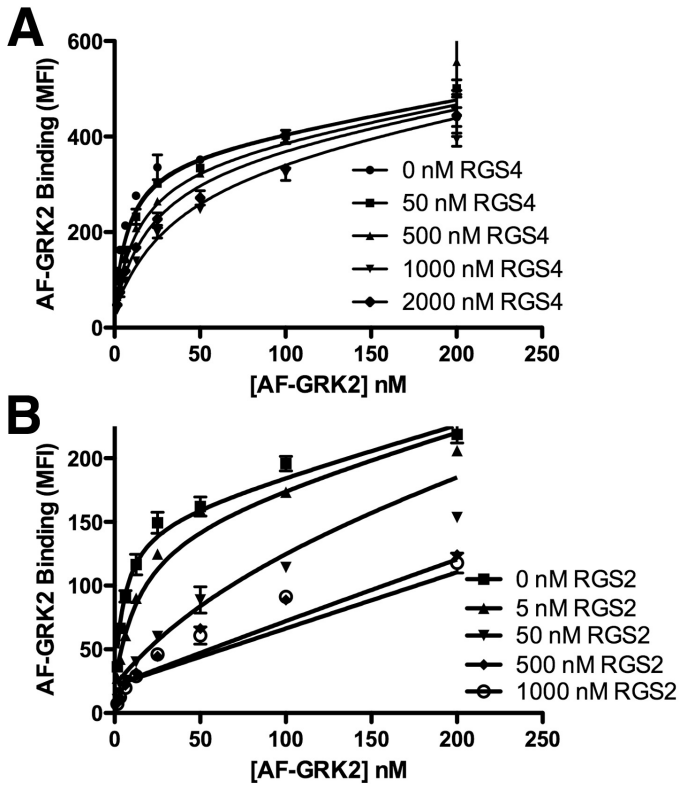

Figure 12: Dose-response curves of AF-GRK2 binding to b-G$\alpha_{i/q}$ are fit poorly by a competitive model. The data in these panels are the same as shown in **Figure 11**A and **Figure 11**B, but Eq. 2 was modified such that [A]/α=0.

Modulation of GAP Activity by GRK2 and p63RhoGEF

The allostery between the RGS and effector binding sites of G$\alpha_{i/q}$ could also manifest itself in the activity of the respective proteins. We therefore tested whether GRK2 and p63RhoGEF could modulate the GAP activity of RGS-Gα_q complexes. GAP assays were performed using the GTPase-deficient G$\alpha_{i/q}$R183C mutant (*114*). Arg183 resides at the beginning of switch I in Gα_q and stabilizes the negative charge on the γ-phosphate of GTP during the transition

state of GTP hydrolysis. Arg183 does not interact with effectors or with RGS proteins in crystal structures, and the $G\alpha_q$ R183C mutant hydrolyses GTP slowly, facilitating measurement of GAP activity, but still activates its effectors PLCβ and p63RhoGEF, binds GRK2, and responds to the GAP activity of RGS proteins (*24, 29, 115*). We first compared the GAP activity of 200 nM RGS2, RGS4 and ΔN-RGS2 (Figure 13A). Under our experimental conditions, $G\alpha_{i/q}$R183C hydrolyzed GTP at a basal rate of 0.004 ± 0.001 min^{-1}. Addition of 200 nM RGS2 stimulated this rate 30-fold, while 200 nM RGS4 produced an 11-fold increase. Despite the lower apparent affinity of ΔN-RGS2 protein for b-$G\alpha_{i/q}\cdot AlF_4^-$ (Table 1), this protein had higher GAP activity than wild-type RGS2 (80-fold over basal).

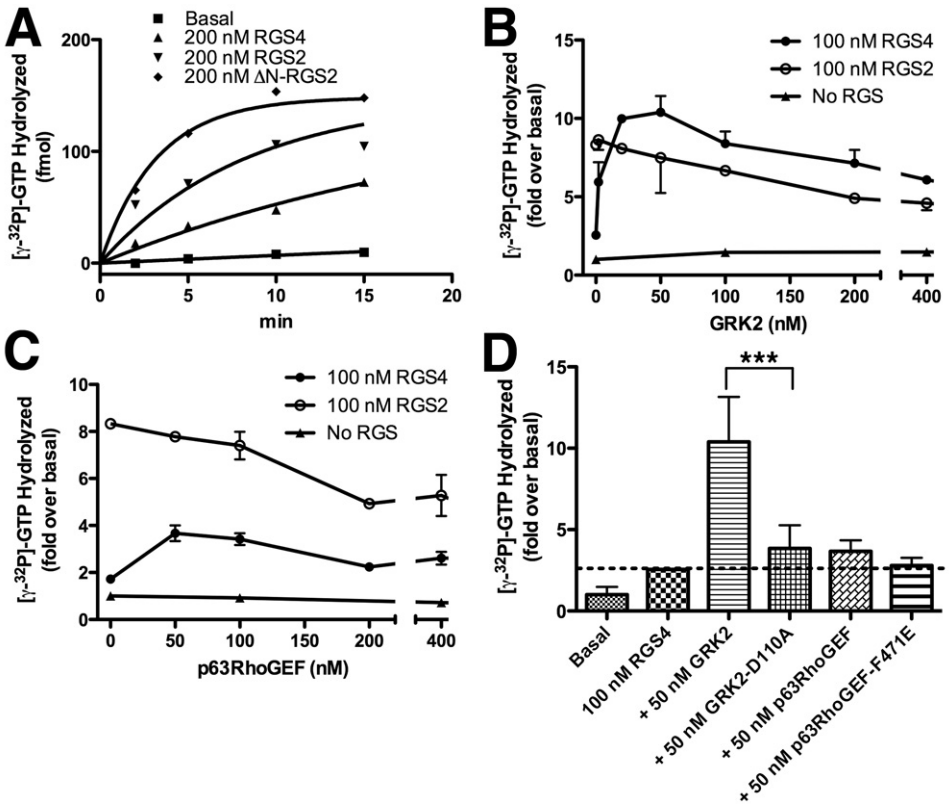

Figure 13: Modulation of GAP activity by GRK2 and p63RhoGEF. Data by Dr. Aruna Shankaranarayanan. **A)** Comparison of the GAP activity of 200 nM of each RGS protein on $G\alpha_{i/q}R183C$. In this experiment, data were fit to a one phase exponential to give rate constants of 0.005 (basal), 0.12 (RGS2), 0.044 (RGS4), and 0.31 (ΔN-RGS2) min^{-1}. **B)** The effect of GRK2 on the GTPase activity of $G\alpha_{i/q}R183C{\cdot}GTP$ in the presence and absence of 100 nM RGS protein. The amount of ^{32}P released at 2, 5, 10, and 15 minutes were quantified and fit to lines. The slopes were then normalized either with respect to basal activity (GRK2 alone curves) or with respect to the 100 nM RGS slope (GRK2 + RGS protein curves). The 20 nM GRK2 time point in the RGS4 curve and the 20 and 200 nM time points in the RGS2 curve are from a single experiment. The remaining time points represent the means ± SD of 2-7 experiments. **C)** The

effect of p63RhoGEF on the GTPase activity of $G\alpha_{i/q}$R183C·GTP in the presence or absence of RGS proteins. The 200 nM time point in the RGS4 curve and the 50 and 200 nM time points in the RGS2 curve are from a single experiment. The remaining time points represent the means ± SD of 3-6 experiments. **D)** The enhancement of RGS4-stimulated GTP hydrolysis by GRK2 and p63RhoGEF is specific. The GRK2-D110A and p63RhoGEF-F471E $G\alpha_q$-binding deficient mutants, used at the same concentrations as their wild-type equivalents, were deficient in stimulating GTP hydrolysis. Data points represent the mean fold over RGS ± SD (n=3). Data were analyzed with a Tukey's post-test. Three asterisks indicates a significant difference between the indicated columns at the $p<0.001$ level.

To avoid saturating the GAP activity, we measured GTP hydrolysis on $G\alpha_{i/q}$R183C using RGS proteins at half the prior concentration (100 nM), at which the apparent rate constants were 0.06 ± 0.02, 0.012 ± 0.001 and 0.16 ± 0.02 min^{-1} for RGS2, RGS4, and ΔN-RGS2, respectively. This also enabled us to measure the RGS-stimulated release of ^{32}P over a 15 min time course with approximately linear kinetics. In the absence of RGS proteins, neither GRK2 nor p63RhoGEF significantly stimulated GTP hydrolysis on $G\alpha_{i/q}$R183C (Figure 13B and C). However, at concentrations up to 50 nM, GRK2 acted synergistically with RGS4 and stimulated the rate of GTP hydrolysis up to a maximum of ~4-fold over RGS4 alone. Smaller magnitude effects were observed with p63RhoGEF in place of GRK2, with the maximal extent of activation being 1.4 fold at 100 nM

p63RhoGEF (Figure 13C). Point mutants of GRK2 and p63RhoGEF that are deficient in binding $G\alpha_q$ (D110A and F471E, respectively) did not similarly enhance the rate of GTP hydrolysis by RGS4 (Figure 13D), indicating that the synergistic effects of 50 nM GRK2 and p63RhoGEF are specific. The 4-fold rate enhancement we measured for RGS4 and GRK2 is similar to that observed for the cooperative interaction of RGS9 and PDEγ with $G\alpha_t$ (*84, 85*). Interestingly, whereas GRK2 and p63RhoGEF appeared to have only small effects on the affinity of RGS4 for $G\alpha_q$ (Figure 9E), PDEγ enhanced the affinity of RGS9 for $G\alpha_t$ (*86*). Obviously, affinity for the $G\alpha_{i/q}{\cdot}AlF_4^-$ state is not completely correlated with GAP activity. In contrast to RGS4, RGS2-mediated stimulation of GTP hydrolysis was not significantly affected at concentrations of either GRK2 or p63RhoGEF up to 100 nM (Figure 13B,C).

At the higher concentrations of GRK2 or p63RhoGEF, the GTP hydrolysis rates mediated by RGS2 and RGS4 gradually decrease. Because 400 nM GRK2-D110A and p63RhoGEF-F471E did not have this effect, (Figure 14), the slow decrease in the rate of GTP hydrolysis appears to require formation of a $G\alpha_q$-GRK2 or $G\alpha_q$-p63RhoGEF complex. Biphasic curves such as that exhibited by GRK2 and RGS4 (Figure 13B) could imply multiple binding sites for GRK2 and p63RhoGEF on $G\alpha_{i/q}$, but this does not seem structurally reasonable. The decrease in GTP hydrolysis was also not dependent on the amino terminus of the RGS protein, as both ΔN-RGS2 and full length RGS2 were inhibited at high GRK2 concentrations (Figure 13B, Figure 14). Because the GAP assay is not

performed at equilibrium, it is possible that the slow decrease in the rate of GTP hydrolysis is due to a decrease in the rate of association of RGS protein at high concentrations of GRK2 or p63RhoGEF (*113*).

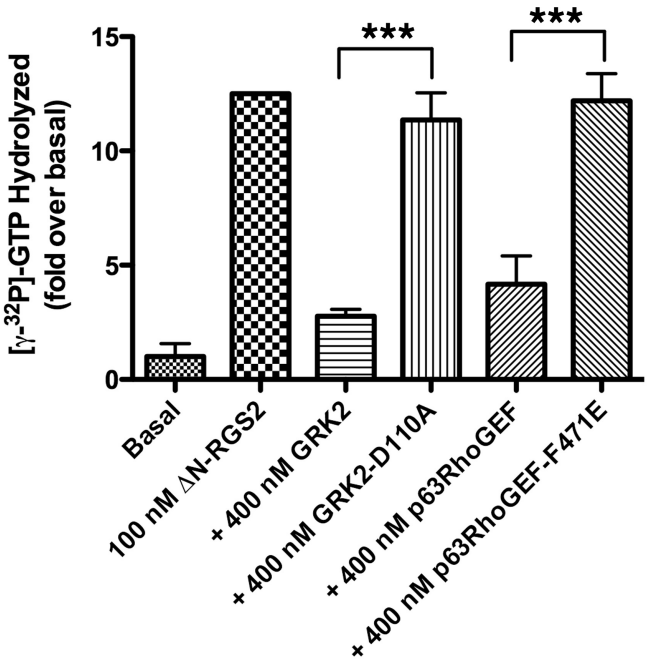

Figure 14: Decrease in RGS2-mediated GTP hydrolysis at higher concentrations of GRK2 and p63RhoGEF is specific. Data by Dr. Aruna Shankaranarayanan. The GRK2-D110A and p63RhoGEF-F471E $G\alpha_q$-binding deficient mutants could not inhibit ΔN-RGS2-mediated GTP hydrolysis to the same extent as their wild-type equivalents. Data points represent the mean fold over RGS ± S.D (n=3). Three asterisks indicates a significant difference between the indicated columns at the ANOVA $p<0.001$ level.

Inhibition of $G\alpha_q$-mediated p63RhoGEF Activity by RGS2 and RGS4

We also tested whether RGS proteins could modulate effector activity in a GAP-independent manner. Although there is no observable increase in GRK2 activity as a function of $G\alpha_q$ that can be readily measured *in vitro* (*29*), we could examine the effect of RGS2 and RGS4 on the $G\alpha_{i/q}{\cdot}AlF_4^-$-stimulated nucleotide exchange activity of p63RhoGEF. In this assay, nucleotide exchange onto RhoA was measured by an increase in fluorescence polarization of a fluorescently labeled GTPγS nucleotide as it binds RhoA. Both RGS4 and RGS2 can dramatically reduce the activity of $G\alpha_{i/q}$-p63RhoGEF (Figure 15). The inhibition was specific, because 2 μM RGS2-N149D and 2 μM RGS4-N128G had no affect on the rate of $G\alpha_{i/q}$-stimulated GEF activity on RhoA. Experiments in which the addition of RGS protein was delayed by one or two hours did not generate differences in inhibition (data not shown), suggesting that the observed loss of exchange activity is not a kinetic artifact due to changes in association or dissociation kinetics. Thus, it appears that RGS proteins are indeed able to modulate the activity of p63RhoGEF through both an allosteric and a GAP mechanism. These data are consistent with reports of RGS2 and RGS4 serving as effector antagonists of PLCβ (*64, 95, 96*). However, because PLCβ possesses its own intrinsic GAP domain (*114*), it is not yet clear whether the antagonism exhibited by RGS proteins against PLCβ will be allosteric or orthosteric.

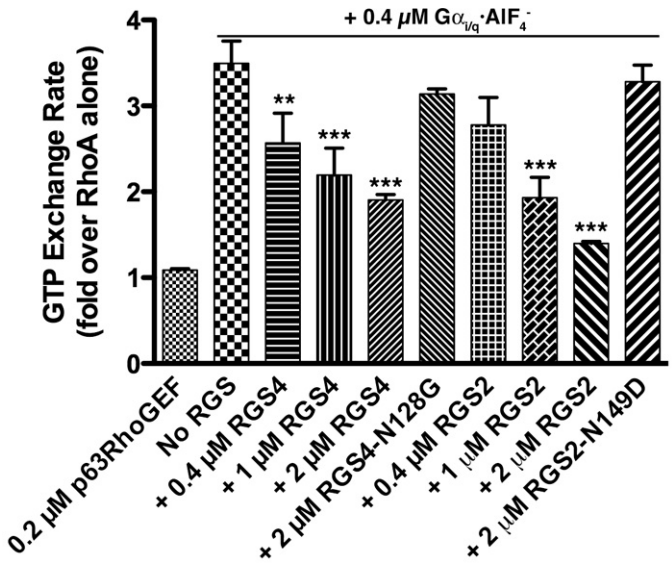

Figure 15: Inhibition of $G\alpha_{i/q}$-stimulated p63RhoGEF activity by RGS2 and RGS4. Data by Dr. Aruna Shankaranarayanan. Nucleotide exchange on RhoA was monitored by the increase in fluorescence millipolarization (mP) of BODIPY FL GTPγS upon binding RhoA. The resulting data were fit as one phase exponentials and are expressed here as the average fold over basal exchange ± SD from three independent experiments, each measured in triplicate. Two asterisks indicate an ANOVA $p<0.01$ and three asterisks an ANOVA $p<0.001$ between the indicated column and the nucleotide exchange mediated by the "No RGS" column.

DISCUSSION

Allosteric Behavior of Ternary Complexes

Positive allosteric behavior was previously observed in the ternary complex formed by $G\alpha_t$, PDEγ and RGS9. Negative allostery was exhibited between

PDEγ and other RGS proteins tested, including RGS4 and RGS16 (*85, 87*). Our data indicates that Gα_q also can form ternary complexes with RGS proteins and proteins that bind at its effector-binding site. In these complexes, both RGS2 and RGS4 negatively modulate the binding of GRK2 to G$\alpha_{i/q}$ (Figure 11). Competition experiments indicated that RGS2 and RGS4 also negatively modulate the binding of p63RhoGEF (Figure 9). The allostery of these ternary complexes also had striking effects on the activity of the RGS and effector proteins. RGS4 GAP activity on Gα_q was potentiated by GRK2 and p63RhoGEF, while that of RGS2 was unaffected or slightly decreased (Figure 11B,C). The Gα_q-stimulated activity of p63RhoGEF was specifically inhibited by both RGS2 and RGS4 (Figure 13). Because Gα_t is a representative member of the Gα_i family, and Gα_q of the G$\alpha_{q/11}$ family, allosteric interplay between the RGS- and effector-binding sites appears possible for all Gα subunits that bind RGS proteins. The most likely conduit for such allosteric communication is the amino terminus of the helix at the beginning of switch II. This region is conformationally responsive to the nucleotide-bound state of Gα and is bracketed by interactions with both RGS protein and effector in the RGS9-Gα_t-PDEγ complex (Figure 5 and Figure 6). This part of switch II also contributes a critical glutamine residue to the hydrolytic site of Gα (*16*). Thus, subtle changes in the conformation of this region could have profound effects on the affinity of effectors and GAPs and on the rate of GTP hydrolysis.

Despite the great structural diversity exhibited by the protein domains that interact with the effector-binding sites of $G\alpha_q$ and $G\alpha_{i/t}$ (Figure 6), the ability to form ternary complexes between effectors, $G\alpha$ subunits and RGS proteins appears remarkably well conserved. What physiological roles might these ternary complexes serve? Segregation of the effector and RGS binding sites on the $G\alpha$ subunit enables RGS proteins to modulate signal transduction of effector-bound $G\alpha$ subunits. This may enable faster rates of signal termination because RGS proteins would not have to compete for the same site as effectors. The enhancement of the GAP activity of RGS9 on $G\alpha_t$ mediated by $PDE\gamma$ is required for physiological rates of signal termination in rod cells. Because of this requirement, the synergy between $PDE\gamma$ and RGS9 has been proposed to be a mechanism that helps to ensure that phototransduction occurs through PDE before GAP activity is brought to bear, preventing a potential short-circuit (*87, 116*). Thus, $G\alpha_t$, $PDE\gamma$ and RGS9 collaborate to achieve both efficient signal tranduction (no short circuit) and high time resolution (rapid GTP hydrolysis on $G\alpha_t$) (*117*). $G\alpha_q$ is the $G\alpha$ subunit responsible for invertebrate phototransduction and, from an evolutionary perspective, may have similar requirements for efficient effector coupling and rapid signal termination. Invertebrate phototransduction is mediated by a phospholipase C enzyme which, like vertebrate $PLC\beta$s, has its own intrinsic GAP domain (*118*). Indeed, vertebrate $PLC\beta1$ can stimulate GTP hydrolysis on $G\alpha_q$ by three orders of magnitude (*119*) to rates similar to the rate of signal termination in invertebrate vision (*120*). The presence of both a GAP and effector in the same molecule ensures both signal

transduction and high time resolution. However, like PDEγ, GRK2 and p63RhoGEF have little or no GAP activity for Gα_q in the absence of RGS proteins. When challenged by RGS4, which can accelerate GTP hydrolysis on Gα_q at even higher rates than PLCβ1 (*119*), a mechanism to avoid a short circuit of the signals passed by p63RhoGEF and, perhaps, GRK2 may become necessary. The synergistic GAP activity exhibited by RGS4 and GRK2/p63RhoGEF could therefore be a mechanism to keep the rates of Gα_q GTP hydrolysis lower unless an effector is already engaged with Gα_q. The fact that RGS proteins can in addition allosterically affect p63RhoGEF activity (Figure 14) is also evidence that RGS proteins can serve a role in tuning, rather than simply squelching, G_q signal transduction. In fact, if Gα_q is indeed rapidly cycled by GPCRs (*16, 93*), then tuning the amplitude of the signal may be the ultimate manifestation of RGS activity on Gα_q.

Differential Allostery Exhibited by RGS2 and RGS4

RGS2 exhibits GAP activity that is not positively cooperative with effector-binding (Figure 13) and has a much stronger negative allosteric effect than RGS4 on the affinity of proteins that bind at the effector-site of Gα_q (Figure 9, Figure 11). Clearly, two different RGS proteins, even members of the same RGS subfamily, can have strikingly different allosteric effects. The ability to form distinct complexes between Gα_q, effectors and RGS proteins with different allosteric properties may ultimately allow for a greater ability to tune the strength and duration of signal transduction to meet the specific requirements of a particular

cell-type or physiological setting. For example, RGS2 may be upregulated by cells in situations when a short-circuit of $G\alpha_q$ signaling would be beneficial.

The Role of GRK2 as a *Bona Fide* $G\alpha_q$ Effector.

GRK2 and p63RhoGEF are similar not only in the manner in which they bind $G\alpha_q$ (Figure 6) but also in the way their binding is allosterically regulated by RGS proteins. Our data therefore supports the idea that GRK2 is a bona fide effector target of $G\alpha_q$ whose activity can potentially be modulated by the action of RGS proteins *in vivo*. Because $G\alpha_q$ as of yet has no obvious effect on the catalytic activity of GRK2 *in vitro* (*29*), the role of $G\alpha_q$ in regulating GRK2 signaling might simply be translocation of the soluble enzyme to cell membrane where its targets are found. Although recruitment of the RGS homology domain of GRK2 to the membrane by activated $G\alpha_q$ has been observed in cells (*27, 121*), membrane translocation of GRK2 has historically been attributed to $G\beta\gamma$ subunits (*122, 123*). Under conditions near physiological ionic strength, GRK2 binds to $G\alpha_{i/q}{\cdot}AlF_4^-$ with >10-fold higher affinity than to $G\beta\gamma$ subunits in detergent micelles (V. Tesmer, unpublished data). $G\alpha_q$ might therefore be the principal route by which GRK2 is recruited to membranes when G_q-coupled receptors are activated, especially if $G\beta\gamma$ were involved in interactions with other peripheral membrane proteins (*e.g.* PLCβ). However, even if $G\beta\gamma$ were solely responsible for membrane translocation of GRK2, RGS-$G\alpha_q$ complexes could still modulate GRK2 activity by controlling how long $G\beta\gamma$ interacts with GRK2. RGS-accelerated GTP

hydrolysis, allosterically tuned by GRK2, would more rapidly return $G\alpha_q$ to its deactivated GDP-bound state, which would then sequester $G\beta\gamma$ from GRK2.

The best-established "downstream" target of GRK2 is of course an activated GPCR. Phosphorylation of these GPCRs recruits arrestin, uncouples G proteins from the receptor, targets the receptor for clathrin-mediated endocytosis, and activates arrestin-mediated pathways. The idea that RGS proteins might regulate this activity is an intriguing one, and suggests that conditions that lead to upregulation of RGS proteins might also lead to a loss of GRK2 and GRK3-mediated phosphorylation of at least $G\alpha_q$-coupled GPCRs. We speculate that this might offer a protective effect against relatively transient changes in cellular environment where a given cell might want to suppress signaling by $G\alpha_q$ yet preserve receptor number and function at the membrane.

Summary

In summary, our data support the idea that RGS proteins are the third component of a ternary complex formed by $G\alpha_i$ and $G\alpha_q$ subunits during active signal transduction. Because GPCRs are also reported to interact with RGS proteins, an activated receptor may be a fourth obligate member of this complex. Not only has nature mandated that effectors and RGS proteins co-exist in complexes with $G\alpha_q$, but also it appears that $G\alpha_q$ subunits have evolved to adopt a specific orientation at the membrane while engaging effectors (Figure 6). This orientation may be conserved for the purpose of promoting productive interaction with

membrane- or receptor-associated RGS proteins, and may also provide the underlying molecular basis for the rapid nucleotide cycling of Gα subunits that occurs in the presence of RGS proteins at activated G_q-coupled receptors (*16, 93*).

FUTURE DIRECTIONS

Our current findings show that ternary complexes can be formed between $G\alpha_q$, RGS2/4, and GRK2/p63RhoGEF in a way that is similar to that of RGS9-$G\alpha_t$-PDEγ. Intriguingly, our data corroborate the hypotheses that both RGS2 is selective for $G\alpha_q$ versus RGS4 and that GRK2 is a *bona fide* effector of $G\alpha_q$. It is well known the RGS2 and RGS4 differ in potency as inhibitors of $G\alpha_q$ versus $G\alpha_i$ signaling (*62, 63*). However, it is not clear mechanistically how the selectivity is achieved. One model suggests that selectivity could be achieved by differences in conformation of the switch I region in $G\alpha_q$ vs $G\alpha_i$. Another model suggests that sequence differences in residues of RGS2 and RGS4 that are implicated in binding an invariant threonine residue in the Gα subunits are responsible for the selectivity. Indeed, mutations of two of these residues (RGS2-C106S and RGS2-N184D) have been shown to increase the binding affinity of RGS2 for $G\alpha_{i1}$ (*62*). Additionally, RGS2-Glu191 has been implicated in selectivity through possible interactions with the α-helical domain on the Gα subunit (*63*). It would be interesting to test these mutations to see if the greater negative allostery of RGS2 could be lessened to that of RGS4. Figure 16 shows the residues in RGS2 and RGS4 that have been implicated in $G\alpha_q$ selectivity (colored purple),

additionally, residues that are in close proximity to effector binding (colored red) could also play a role in the observed allostery due to steric hindrance towards effector binding.

The simultaneous association of $G\alpha_q$ and $G\beta\gamma$ with GRK2 is a feature that is shared with other classic effectors such as adenylyl cyclase and PLCβ. To date no signaling pathway has been attributed to $G\alpha_q$ mediated activation of GRK2, although, GRK2 has been shown to phosphorylate IRS-1 (*90*), ezrin (*92*), p38 MAP kinase (*91*) in response to activation of G_q-coupled receptors. Indeed, the role of the $G\alpha_q$-GRK2 activation may simply be regulating the phosphorylation of GPCRs by helping to recruit GRK2 to the membrane. Another possible future direction would therefore be to determine if RGS interactions with $G\alpha_q$ are capable of regulating phosphorylation of GPCRs by GRK2 providing a novel alternative pathway for differential handling of feedback inhibition and longer term regulation.

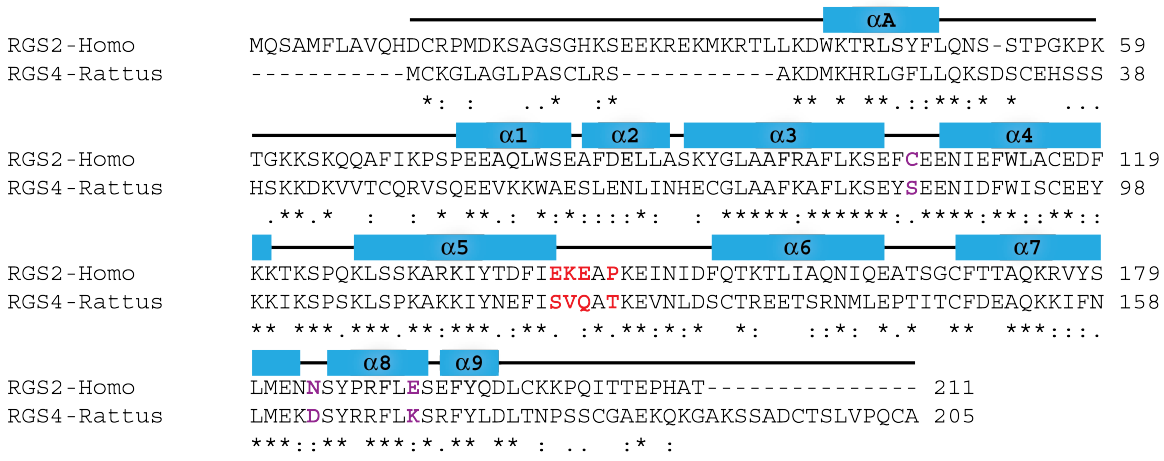

Figure 16: Sequence alignment of RGS2 and RGS4. Sequence alignment of human RGS2 and rat RGS4 was performed using Clustalw

(www.ebi.ac.uk/clustalw). The secondary structure α-helices are shown as blue cylinders labeled as α1-α9 for the traditional helices based on the RGS4 structure and αA for the amphipathic helix in the N-terminal region of RGS2. Residues colored in purple have been shown in the literature to be important in the selectivity of RGS2 versus RGS4 for the binding of $G\alpha_q$ (*62, 63*). Residues colored in red are located in the α5-α6 loop and come into the closest contact with the effector binding site (based on GRK2/p63RhoGEF).

Chapter 3
Screening for Small Molecule Inhibitors of the $G\alpha_q$-GRK2 Protein-Protein Interaction

BACKGROUND AND PROJECT GOALS

Physiological Roles of $G\alpha_q$ and GRK2

The heterotrimeric G protein G_q ($G\alpha_q\beta\gamma$) is a key regulator of cardiovascular development and function. Signaling through G_q-coupled receptors is responsible for regulating a diverse range of responses in the cardiovasculature including platelet activation (*20*), heart development, and cardiac hypertrophy (*124-128*). The classic downstream effector of the $G\alpha_q$ subunit is phospholipase Cβ (PLCβ). Activation of PLCβ leads to the hydrolysis of membrane bound phosphotidylinositol-bisphosphate (PIP_2) into diacylglycerol (DAG) and inositol 1, 4, 5-triphosphate (IP_3), which leads to activation of the protein kinase C pathway (Figure 17). It is now known that $G\alpha_q$ also interacts with other effector enzymes including a family of RhoA mediated nucleotide exchange factors. This includes p63RhoGEF (*112, 129*), which uses its catalytic Dbl homology domain (DH) to catalyze the nucleotide exchange of RhoA, consequently causing cytoskeleton rearrangements and gene transcription (Figure 17).

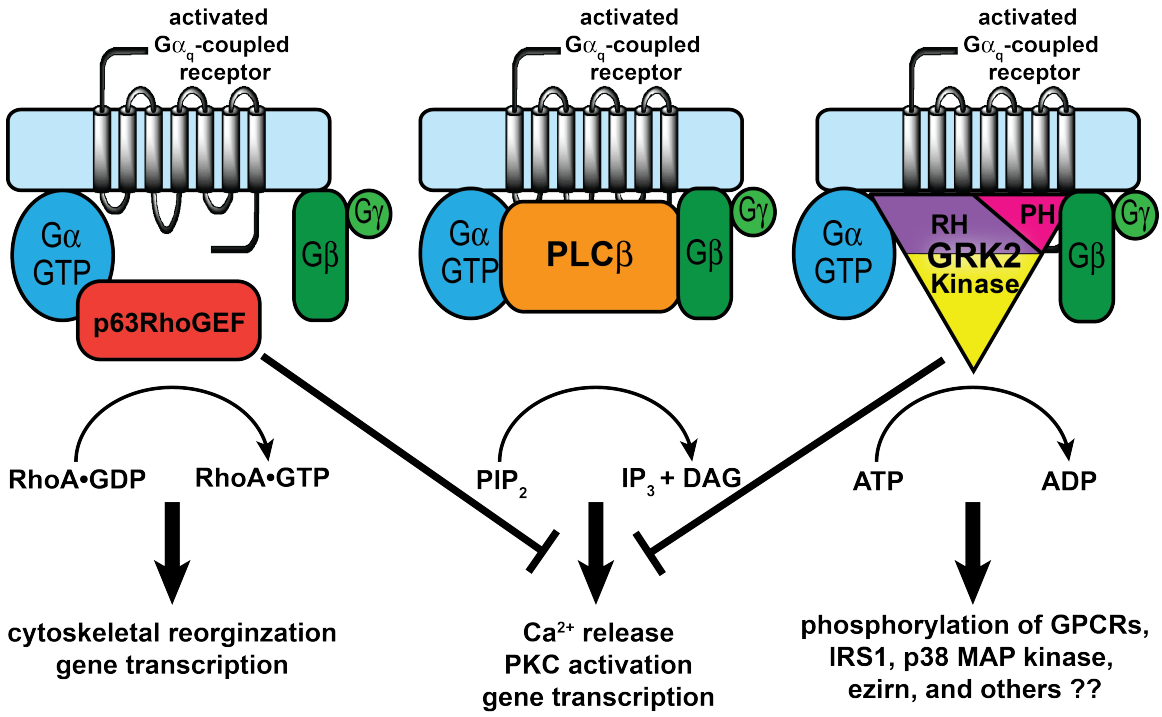

Figure 17: Signal transduction through G_q-coupled receptors. After activation of a G_q-coupled receptor, $G\alpha_q$·GTP dissociates from $G\beta\gamma$ and the two proteins can engage downstream effector targets. All three effectors have distinct downstream targets and sometimes two different $G\alpha_q$ effectors are required for a proper physiological response. Despite this, both GRK2 and p63RhoGEF have been shown to compete with PLCβ for $G\alpha_q$ in overexpression studies. Thus, it is unclear if endogenous effectors compete with each other, or if different effectors are sequestered via scaffolding with distinct receptors. Chemical inhibitors of specific effector interactions would help answer these and other questions about $G\alpha_q$ function in cells.

In addition to PLCβ and p63RhoGEF, there is increasing evidence that GRK2 not only inactivates GPCRs, but also plays a role as a $G\alpha_q$ effector (Figure 17) (*29*).

GRK2 is well known for its role in phosphorylation independent attenuation of GPCR signaling by sequestering activated $G\alpha_q$ subunits (*67-71*). The crystal structure of $G\alpha_q$-GRK2-$G\beta\gamma$ (*26*) confirmed that GRK2 binds $G\alpha_q$ at the effector-binding site. Furthermore, as shown in Chapter 2, GRK2 and p63RhoGEF allosterically regulate $G\alpha_q$-RGS interactions in a similar manner (*130*). Thus, GRK2 is potentially a *bona fide* effector of $G\alpha_q$. However, the exact physiological significance of their interaction is not clear. The obvious role of GRK2 is phosphorylation of GPCRs, and its association with $G\alpha_q$ may simply facilitate recruitment of GRK2 to the cell membrane, although such translocation has generally been attributed to $G\beta\gamma$ (*122, 123*). GRK2 has also been observed to phosphorylate non-receptor targets such as insulin receptor substrate 1 (IRS-1) (*90*), p38 MAP kinase (*91*), and ezrin (*92*) in response to activation of $G\alpha_q$-coupled receptors, consistent with the role of GRK2 as a signal transducing $G\alpha_q$ effector. Thus, there is emerging evidence that GRK2 phosphorylates many other non-GPCR substrates, and associates with a variety of other proteins all involved in various signal transduction pathways (*131*). Indeed, protein interactions surrounding GRK2 have become increasing complex granting GRK2 its own "interactome" and implicating GRK2 in numerous pathologies (*131*). Small molecule inhibitors that could specifically inhibit the binding of $G\alpha_q$ to GRK2 would provide a powerful pharmacological tool for understanding the functions of this interaction.

Protein-Protein Interaction Inhibitors

Discovering small molecule inhibitors that disrupt protein-protein interactions (PPIs) is generally considered very challenging. One of the major difficulties involved in targeting PPIs is the large contact surfaces involved (typically 1,500 – 3,000 $Å^2$) versus those in a protein-small molecule interactions (300-1,000 $Å^2$) (*132-134*). Additionally, the contact surfaces of PPIs are often flat and devoid of grooves and pockets that promote the favorable binding of small molecules. Furthermore, high-throughput screening (HTS) has a poor track record for discovering small molecule inhibitors of protein-protein interactions (*135, 136*). Despite these difficulties, major advances have been made towards discovering small molecule inhibitors of PPIs. One of the first discoveries that opened up the idea was the identification of "hot spots" at protein-protein interfaces (*137, 138*). In "hot spots", the majority of the binding energy of a PPI is contributed to a small subset of amino acids clustered at the center of the interface. In principle, targeting these "hot" amino acids with small molecules would cause disruption of the entire interface (*139*). For example, a "hot spot" on $G\beta\gamma$ was discovered by utilizing a peptide phage display library, which identified a peptide (SIRK) that bound near the center of the interaction surface for both $G\alpha$ subunits and GRK2. A crystal structure between $G\beta\gamma$ and SIRK was then used as the basis for a virtual screen that ultimately indentified a set of compounds that could selectively modulate $G\beta\gamma$ PPI's (*140-142*).

Interaction of $G\alpha_q$ with GRK2

The $G\alpha_q$-GRK2 interface buries an accessible surface area of ~1700 $Å^2$ (*26*), and mutational analysis has revealed several critical residues at the interface that are important for binding (*26*). At the GRK2 interface, residues along the α5 helix of GRK2 dock into a small groove created between the α2-α3 helices of $G\alpha_q$ (Figure 18B,C). Residues 261-263 of $G\alpha_q$ are important for the $G\alpha$ specificity of GRK2 (*26*), but perhaps more importantly these residues bind in a small pocket at the GRK2 interface that could potentially be targeted with small molecule inhibitors and abrogate $G\alpha_q$-GRK2 binding. Furthermore, these residues have an accessible surface area of approximately 305 $Å^2$, which is in line with surface area buried by small molecules. Alternatively, we could identify small molecule inhibitors that bind elsewhere on the RH domain of GRK2 that change the interface allosterically. It is known from our structures that the region of GRK2 that binds $G\alpha_q$ is conformationally flexible, and thus could adapt to bind small molecules.

Mutation of GRK2 residues Arg106, Phe109, Asp110, and Leu118 (Figure 18C, residues colored purple) abolish GRK2 binding to $G\alpha_q$ (*27, 75*) and contribute an accessible surface area of 364 $Å^2$. These critical residues not only bind in a hydrophobic pocket on $G\alpha_q$, but also help in creating a shallow pocket on the surface of GRK2 where residues 261-263 of $G\alpha_q$ bind. The surface area between residues 106-110 of GRK2 and 260-263 of $G\alpha_q$ form a potential “hot spot” that appears to be suitable for small molecule inhibitors. It is certainly

reasonable that we may discover small molecules inhibitors that generically inhibit $G\alpha_q$ by binding into the groove of the effector-binding site. However, such inhibitors are likely to be non-selective and may have limited use.

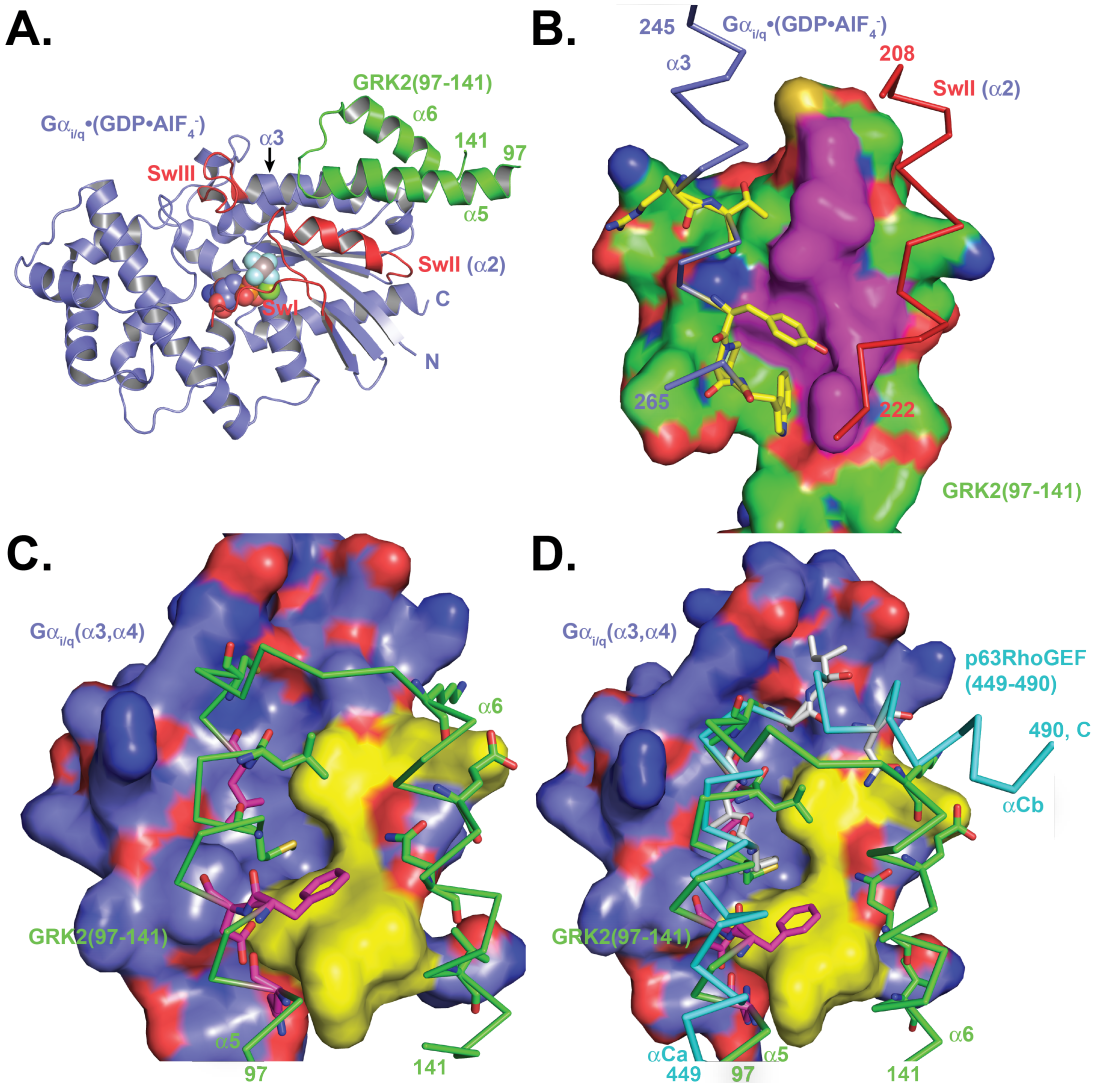

Figure 18: The $G\alpha_q$-GRK2 interface. A) Structure of activated $G\alpha_q$ binding to the RH domain of GRK2. $G\alpha_q$ is colored slate, with the SwII helix colored red. Residues 97-141 of GRK2 are colored green. **B)** A surface view of the GRK2 interface. Residues colored purple on the GRK2 interface are important for

binding to $G\alpha_q$, while residues colored yellow on $G\alpha_q$ are important for binding to GRK2. Switch II residues are also likely to be important for effector binding, however, mutation of these residues leads to a loss of function. **C)** A surface view of $G\alpha_q$ with the α5-α6 helices of GRK2. The α5 helix of GRK2 binds into a small groove on $G\alpha_q$. **D)** Analogous effector interaction with p63RhoGEF binding $G\alpha_q$. Residues colored white on p63RhoGEF are important for binding $G\alpha_q$. Both p63RhoGEF and GRK2 utilize the same hydrophobic groove on $G\alpha_q$ for binding, thus inhibitors that bind $G\alpha_q$ are likely to be unselective.

To our knowledge, there are no known small molecule PPI inhibitors (PPIIs) available for Gα/effector interactions (*134*). However, $G\alpha_q$ is an established target. A $G\alpha_q$ specific inhibitor, YM-254890, was discovered based on its ability to inhibit platelet aggregation (*143*). YM-254890 is a cyclic depsipeptide that inhibits the GDP/GTP exchange on $G\alpha_q$ by inhibiting the release of GDP. The crystal structure of YM-254890 bound to $G\alpha_q\beta\gamma$ revealed that the compound binds in a hydrophobic cleft (not the active-site) between the interdomain linkers connecting the GTPase and helical domains of $G\alpha_q$ (*144*). YM-254890 has certainly proved valuable, given the increasing number of associated publications, but its functionality is limited since it blocks all downstream $G\alpha_q$ interactions. We are thus primarily interested in small molecules that inhibit $G\alpha_q$-GRK2 by binding to GRK2. Supporting this idea are several recently discovered PPIIs of the RGS4-$G\alpha_o$ interaction (*102, 145-150*). Like GRK2, RGS4 has a structurally related RH domain, which binds Gα subunits. Furthermore, one of

the RGS4 inhibitors was discovered by HTS using the flow cytometry protein interaction assay (FCPIA) (*102, 151*), an assay that has served as my workhorse for much of this thesis (*130*).

Project Goals

The importance of $G\alpha_q$ and GRK2 in regulating cardiovascular function is well documented. Both proteins are implicated in the development of cardiac disease and hypertension. Determining the specific role of the $G\alpha_q$-GRK2 interaction may help us come to a complete understanding of cardiac physiology and disease, and may open up new avenues for therapeutic intervention. Small molecule inhibitors that selectively inhibit this interaction would potentially serve as powerful pharmacological tools. While the identification of PPIIs is a challenging goal, small molecules have been discovered that target both $G\beta\gamma$ subunits and RGS4. Therefore, the identification of compounds that selectively target the $G\alpha_q$-GRK2 interface should be feasible.

METHODS

Purification of $G\alpha_q$

A $G\alpha_{i/q}$ chimera containing the amino terminal helix (residues 1-28) of $G\alpha_i$ joined to the remainder of mouse $G\alpha_q$ (37-359) was purified as previously described (*26*), with one notable exception: $G\alpha_{i/q}$ was co-expressed with mammalian Ric-8A. Ric-8A is a non-receptor GEF (*30, 152*) for most $G\alpha$ subunits (excluding

$G\alpha_s$) and co-expression of Ric-8A with $G\alpha$ subunits dramatically increases protein yields (Personal Communication, Gregory Tall). Baculovirus for co-expression of Ric-8A with $G\alpha_{i/q}$ was a gift from Stephen Sprang (University of Montana).

Purification of GRK2

GRK2-S670A was purified as described before (*100*). The S670A mutation removes a MAP kinase phosphorylation site (*153*), which has no influence on *in vitro* kinase activity or $G\alpha_q$ binding.

Preparation of Screening Reagents

Alexa Fluor 488 labeling of $G\alpha_q$

$G\alpha_q$ was fluorescently labeled using the thiol-reactive probe Alexa Fluor 488 C_5 maleimide (AF-488; Invitrogen, #A-10254). Before fluorescent labeling, $G\alpha_q$ was buffer exchanged into 20 mM HEPES pH = 8.0, 150 mM NaCl, and 50 μM GDP (no DTT) using a Micro Bio-Spin 6 chromatography column (BioRad). A 3-fold molar excess of AF-488 was added to $G\alpha_q$ and allowed to react for 1 hour at 4°C in the dark. The reaction was quenched by supplementing with 2 mM DTT, and the labeled protein was purified from excess fluorophore using a Micro Bio-Spin 6 chromatography column. Protein concentration was determined by spectrophotometric analysis (A_{280}) correcting for AF-488. Fluorescently labeled $G\alpha_q$ is henceforth referred to as AF-$G\alpha_q$.

Biotinylation of GRK2

GRK2 was biotinylated using a 3-fold molar excess of amine-reactive N-hydroxysuccidimyl ester (Sigma, #H1759). The reaction was incubated for 1 hour at 4°C, and was quenched with 10-fold molar excess of glycine. Unbound biotin was removed using a Micro Bio-Spin 6 chromatography column, and the protein concentration was determined by A_{280}. Biotinylated GRK2 is henceforth referred to as bGRK2.

Flow Cytometry Protein Interaction Assay

$G\alpha_q$-GRK2 Binding Assay

Equilibrium binding experiments between $G\alpha_q$ and GRK2 were performed as previously described (*130*), with modifications. Briefly, streptavidin polystyrene beads (2.0-2.9 μm; Spherotech, #SVP-20-5) were vortex mixed, and diluted into 1 mL of –AMF buffer that contains: 50 mM HEPES pH=8.0, 100 mM NaCl, 0.1% lubrol, 5 mM $MgCl_2$, 1% BSA, 2 mM DTT, and 50 μM GDP. The beads were pelleted (2 min, 8K RPM), supernatant removed, and resuspended into 1 mL of –AMF buffer a total of three times. The beads were then resuspended into 500 μL of –AMF buffer, and bGRK2 was added such that its final concentration was 5 nM. The beads were incubated at room temperature for 30 min and subsequently washed three times. Beads were then resuspended in –AMF buffer to their final assay volume (~5mL for one 96-well plate). During the bead incubation, AF-$G\alpha_q$ was prepared. Activation buffer (+AMF) for AF-$G\alpha_q$ was

prepared by adding 20 μM $AlCl_3$ and 10 mM NaF (final concentrations) to –AMF buffer. Concentrated AF-Gα_q was diluted into both –AMF and +AMF buffers to achieve the inactive and activated states of Gα_q, respectively. AF-Gα_q diluted in –AMF buffered served as our background control for the assay. AF-Gα_q was then serially diluted down a 96-well PCR plate to yield AF-Gα_q concentrations generally between 0.78 and 100 nM. Subsequently, 50 μL of bead bound bGRK2 was added to each well of the 96-well plate. The proteins were incubated for ~30 minutes at room temperature in the dark before being read on Accuri C6 flow cytometer (Accuri Cytometers, Ann Arbor, MI) that was attached to a HyperCyt Autosampler (IntelliCyt, Albuquerque, NM). Median fluorescence intensity was calculated and used for data analysis. Data was fit to a one-site total and nonspecific-binding curve using Prism 5.0.

Z-factor Determination

Z-factor for our assay was determined using the following equation:

$$Z - factor = 1 - \frac{3 \times (\sigma p + \sigma n)}{|\mu p - \mu n|}$$

where σ represents the standard deviation of the positive and negative (p, n) controls and μ represents the mean of the positive and negative control values. Positive controls were determined using 192-wells containing 5 nM of –AMF Gα_q and negative controls were determined using 5 nM of +AMF Gα_q. In our system the positive controls represent full inhibition (0% bound) and the negative

controls represent no inhibition (100% bound). Z-factors were determined in the presence of 1% DMSO to emulate screening conditions.

Primary HTS Protocol

The protocol for our primary screening assay was adapted from previous HTS campaigns that used FCPIA to screen for small molecule inhibitors against RGS4-$G\alpha_o$ (*102, 151, 154*). Our screen was run in collaboration with the Center for Chemical Genomics (CCG) at the University of Michigan against ~40,000 compounds from the following chemical collections: MS Spectrum 2000, ChemDiv, Maybridge HitFinder, CMLD, and the BioFocus NCC. In brief, 0.2 μL of each compound was transferred into 10μL of bead bound bGRK2 using a Beckman BioMek XL liquid handling robot. Next, 5μL of AF-$G\alpha_q$ in –AMF buffer was added to every well of a 384-well plate (Costar, #3676) for a final concentration of 5 nM AF-$G\alpha_q$. We subsequently added 5 μL of –AMF buffer to columns 23/24 and 5 μL of +AMF buffer to columns 1-22. Plates were incubated at room temperature for 30 min, and then read on the Accuri-HyperCyt. The final concentration of DMSO for the assay was 1% with a compound concentration of ~10 μM. Our assay format consisted of columns 1/2 as the negative control wells, columns 3-20 as the compound wells, and columns 23/24 as the positive control wells. Data was binned and analyzed using HyperView software, and subsequently uploaded to the MScreen database. The assay had a throughput of 10-20 plates per day.

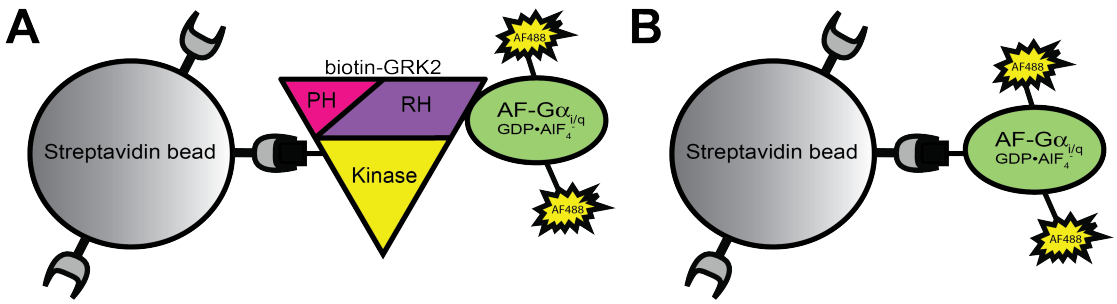

Figure 19: HTS using FCPIA. A) Schematic of the Gα_q-GRK2 interaction using FCPIA. Biotinylated GRK2 is immobilized on streptavidin beads. Bead-bound fluorescence associated with AMF-activated Gα_q binding GRK2 is measured via identification of the bead and the associated fluorescence of AF-488 using an Accuri C6 flow cytometer. The binding affinity for activated Gα_q-GRK2 is ~5 nM (see Chapter 2). **B)** Schematic of the biotin/AF-Gα_q counter-screen. The biotin/AF-Gα_q counter-screen was used to eliminate compounds that non-specifically interact with the assay.

Dose-Response Titrations and Counter-screening

Dose-response titrations were run in parallel with a fluorescent counter-screen that consisted of biotinylated AF-Gα_q (biotin/AF-Gα_q) immobilized on streptavidin beads (Figure 19B). Compounds were serially diluted by a factor of 3.16 in 10μL of +AMF buffer with a final concentration range of 100 μM to 31.6 nM. Biotinylated GRK2 (5 μL) and either AF-Gα_q (5 μL) or biotin/AF-Gα_q (5 μL) was subsequently added to each well, and bead-bound fluorescence was measured as described for the primary screen.

RESULTS AND DISCUSSION

Development of a High-Throughput Screen for the $G\alpha_q$-GRK2 Interaction

FCPIA is readily adaptable for HTS. We have previously used FCPIA to measure protein-protein interactions including the $G\alpha_q$-GRK2 interaction (Chapter 2, (*103, 112, 130*)). Prior to screening, instrumentation changes were made requiring the re-optimization of FCPIA. Most notably, we switched to fluorescently labeling $G\alpha_q$ and biotinylating GRK2 (Figure 19A). Binding of $G\alpha_q$ to GRK2 was retested under our new conditions yielding a K_d value of 6.6 ± 2.7 nM (n=7, in duplicate) similar to our previously determined value of 3.2 ± 1.7 nM (Figure 20A).

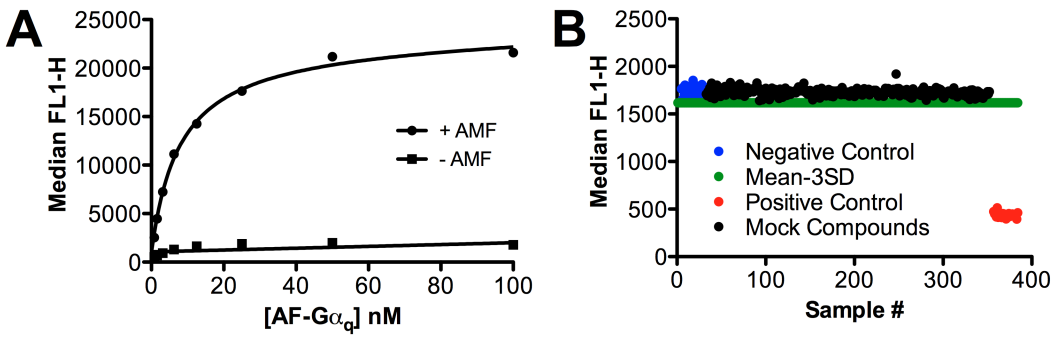

Figure 20: Assay development for HTS of $G\alpha_q$-GRK2. A) Direct binding of AF-$G\alpha_q$ to bGRK2. The binding affinity of the AF-$G\alpha_q$/bGRK2 interaction is 6.6 ± 2.7 nM. Data shown is mean ± SEM representative of 1 of 7 experiments in duplicate. **B)** Z-factor determination for $G\alpha_q$-GRK2. AF-$G\alpha_q$ (5 nM) was added to bGRK2-bound beads. The positive control consists of –AMF $G\alpha_q$. A Z-factor of 0.85 was calculated for the shown experiment. The false positive hit rate of the assay is less than 0.1%.

To determine if our assay was suitable for HTS we determined a Z-factor over several experiments. The Z-factor is a statistical parameter that is defined by the means and standard deviations of the positive and negative controls. In practice, a Z-factor between 0.5 and 1.0 is desirable for screening (*155*). We choose to use 5 nM AF-$G\alpha_q$ in our assay as it is reasonably close to its K_d value, increasing our chances of finding an inhibitor and allowing us to minimize consumption of the most expensive reagent. The calculated Z-factors for our assay were between 0.8 and 0.9 and tested over a period of up to 16 hours, over multiple protein batches (Figure 20B). Overall, the high affinity of the $G\alpha_q$-GRK2 interaction in the presence of AlF_4^- and the low background fluorescence were very suitable for HTS.

Primary Screening Results for Inhibitors against $G\alpha_q$-GRK2

We first performed a small pilot screen in the CCG against the MicroSource Spectrum 2000 compound library (MS2000), which includes FDA approved drugs. Our Z-factor for the collection was ~0.85 over 7 plates with a signal-to-noise of ~5.6. A hit criteria of ≥15% inhibition per plate and a standard deviation per plate ≥ 3.0 resulted in 4 active compounds from the MS2000 library yielding an initial screening hit rate of 0.2%. However, 3 of the 4 actives were immediately removed from follow up analysis, as one compound was highly promiscuous, and the other two compounds were biotin and gentian violet, which were of no further interest. Based on the success of the pilot screen, we screened an additional ~38,000 compounds.

Data from the primary screen was triaged in collaboration with the Medicinal Chemistry Core Synthesis Lab (MCCSL) to select compounds for testing in dose-response titrations. The first criterion were compounds with a percent inhibition by plate greater than or equal to 15%, which resulted in 115 active compounds. The second criterion for actives was a standard deviation (calculated using negative controls and samples) by plate of greater than or equal to 3. This criterion produced an additional 96 active compounds. The last criterion used an activity cutoff for each plate that was defined as the negative control median value minus 6 times the standard deviation (calculated using only the negative control). A compound was considered active if its value was than or equal to the activity cutoff. This criterion resulted in an additional 32 active compounds. The active criteria produced a total of 243 active compounds, three of which were eliminated as described (from the MS2000 screen) yielding a primary screen hit rate of 0.6%.

Elimination of False Positive Hits

To cull out false positive hits, we tested our 240 active compounds simultaneously in dose-response titrations (Figure 21A) and in a fluorescence counter-screen (Figure 21B). For the dose-response titrations we used an IC_{50} value cut-off of less than or equal to 100 μM which produced 75 active compounds. We then excluded compounds which had an IC_{50} value of less than or equal to 100 μM in the fluorescent counter-screen. This resulted in 48 active

compounds, with 13 having an IC_{50} value between 1 and 10 μM, and the remaining compounds having an IC_{50} value over 10 μM.

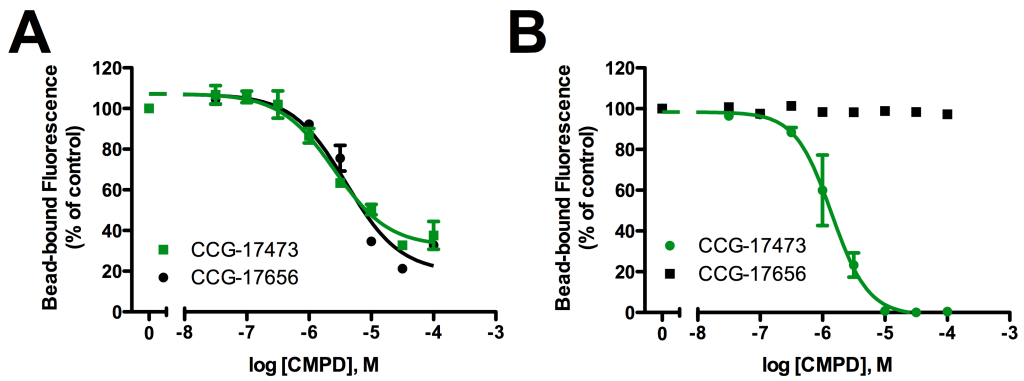

Figure 21: Dose-response titrations against $G\alpha_q$-GRK2. A) Example of two compounds with activity in dose-response titrations. CCG-17473 and CCG-17656 both have an IC_{50} value of approximately 10 μM. **B)** Fluorescent counter-screen results for CCG-17473 and CCG-17656. CCG-17473 is active against biotin/AF-$G\alpha_q$ and was removed from further analysis. The results show mean ± SEM run in duplicate.

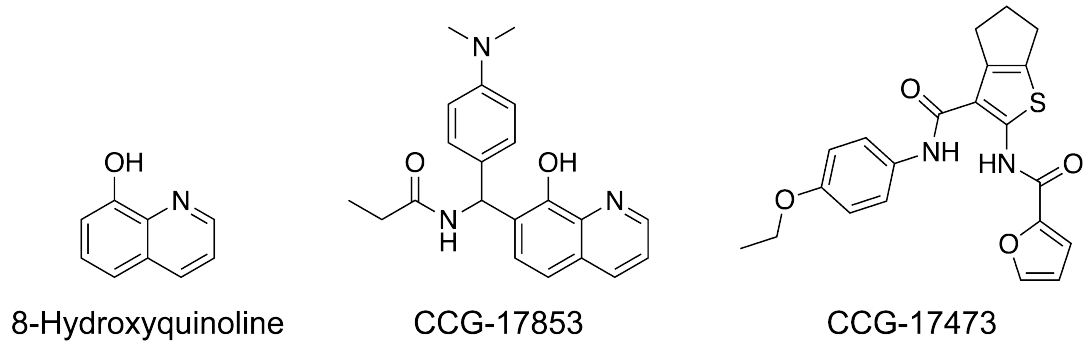

Figure 22: Summary of active compounds from the $G\alpha_q$-GRK2 screen. CCG-17853 is one of 12 other compounds that contain 8-hydroxyquinoline, a known high-affinity chelator of aluminum. CCG-17473 was found to be active in the biotin/AF-$G\alpha_q$ counter-screen and was excluded from further analysis. CCG-42010 was tested in follow-up dose-response titrations using the CCG stock, however, its IC_{50} was well over 100 μm suggesting that it is an artifact. CCG-17656 was reordered, but failed to show activity in follow-up dose-response titrations. CCG-18939 is active in follow-up dose-response titrations, but is a non-specific inhibitor likely due to its catechol group.

We tested 10 of the 48 compounds in follow-up dose-response titrations, including CCG-17853, CCG-17656, and CCG-42010 (Figure 22). Only CCG-42010 had activity, but its IC_{50} value was over 100 μM suggesting that the compound is a non-specific inhibitor. A substructure search revealed that 12 of the 48 compounds contain an 8-hydroxyquinoline group (Figure 22). 8-hydroxylquinoline is well-known chelator of aluminum (*156-159*), and is likely inhibiting $G\alpha_q$-GRK2 by removing aluminum, which is needed to form $GDP{\cdot}AlF_4^-$ and active $G\alpha_q$. Thus, the 8-hydroxyquinoline containing compounds (ex. CCG-17853; Figure 22) were removed from further consideration.

We ranked the remaining 34 active compounds by their potency and efficacy in dose-response titrations. The efficacy of the majority of the compounds is very weak with an inhibition of less that 20% at 100 μM dose of compound. As such,

we ordered our 10 best compounds from their respective vendors and retested them in dose-response titrations. Only one of the reordered compounds, CCG-18939, had activity in further dose-response titrations (Figure 23A). CCG-18939 also displayed similar activity against another Gα-effector interaction, $G\alpha_{13}$-LARG (Figure 23B). Furthermore, CCG-18939 also had strong inhibition against RGS4 in a FRET assay, specifically on the donor fluorophore signal (data not shown, from Mscreen database). Given these results, it is tempting to suspect that CCG-18939 is a non-selective Gα inhibitor. However, CCG-18939 contains a catechol group, which is not only oxidizing and capable of changing colors and inhibiting fluorescence, but is also able of chelating aluminum ions (*160*). CCG-18939 is also active in a total of 8/56 CCG assays and when combined with its relatively high IC_{50} value, it is most likely that CCG-18939 is a non-specific inhibitor.

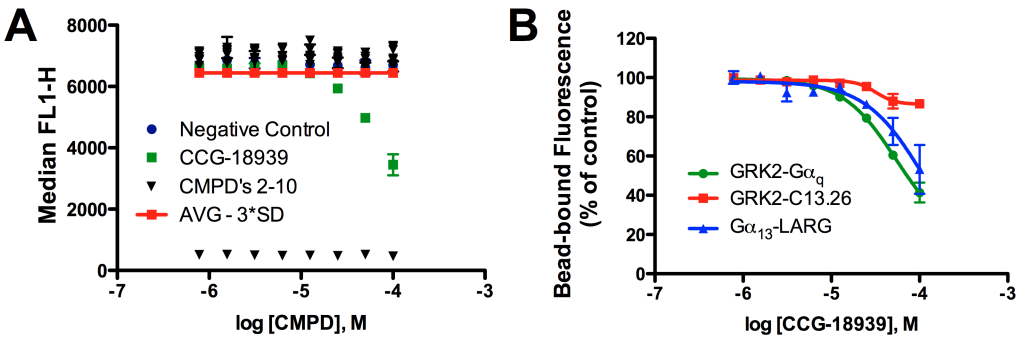

Figure 23: Follow-up activity of our ten best hits. **A)** Dose-response titrations against ten reordered CCG compounds. Only CCG-18939 had activity below three standard deviations from the control (red line). **B)** Dose-response

titrations of CCG-18939 against GRK2-$G\alpha_q$, $G\alpha_{13}$-LARG, and GRK2-C13.26. CCG-18939 has an IC_{50} value of ~75 μM against both GRK2-$G\alpha_q$, and $G\alpha_{13}$-LARG. The results show mean ± SEM run in duplicate.

DISCUSSION

PPIs play a key role in the regulation of almost every biological process. As such, there has been much interest in inhibiting PPIs for their potential therapeutic value. The prevailing view in literature indicates that targeting PPIs with small molecule inhibitors is a formidable challenge. However, much progress has been made over the past 5 years in discovering small molecule inhibitors that specifically inhibit PPIs. Many of the currently discovered small molecule inhibitors of PPIs come from interactions where the α-helix of one protein binds into a well-defined binding pocket of its partner protein (*161*), similar to the docking of the α5 helix of GRK2 into the $G\alpha_q$ effector binding site . Recent examples of successfully targeted protein/peptide-protein interactions include the JNK/JIP interaction (*162*), phospho-peptide/PLK-1 PBD interaction (*163*), the Calcineurin/NFAT interaction (*164, 165*), the SIGK/G$\beta\gamma$ interaction (*140*), and the p53/MDM2 interaction (*166*). The majority of these interactions were screened against using a fluorescence polarization (FP) assay, however, FP requires the use of an isolated peptide-binding domain, which is currently lacking for the $G\alpha_q$-GRK2 interaction. Instead, we chose to use FCPIA to develop a high-throughput screen against the $G\alpha_q$-GRK2 interaction. FCPIA has been previously shown to be useful for studying PPIs, and has been previously

used as a screening platform to discover small molecule inhibitors of RGS proteins against $G\alpha_o$ (*102, 151, 154*).

In our $G\alpha_q$-GRK2 screen, we indentified 243 primary screen hits, which was narrowed down to 48 compounds after dose-response titrations and use of a fluorescent counter-screen (Figure 21B). Out of the 48 compounds, 20 were tested for follow-up activity, with two compounds, CCG-42010 and CCG-18939 having additional activity (Figure 22). However, CCG-42010 has a relatively high IC_{50} value that is well over 100 μM. Additionally, CCG-42010 has activity in 18 out of the 44 primary screen assays run in the CCG, suggesting that this compound is a promiscuous inhibitor. Our other identified compound, CCG-18939, also suffers from a relatively high IC_{50} value of ~75 μM (Figure 23A). Furthermore, CCG-18939 inhibits both $G\alpha_{13}$-LARG and $G\alpha_o$-RGS4 (Figure 23B), and this could be a weak aluminum chelator due to its catechol group (*160*).

Overall, our screening results failed to identify a small molecule inhibitor of $G\alpha_q$-GRK2. We attribute the failure of the screen to the overall difficulty of inhibiting protein-protein interactions and not to poor assign design. Current small molecule libraries are generally not designed towards inhibiting protein-protein interactions as they are come from compounds designed towards targeting enzyme active sites. In fact, a majority of the currently described small molecule PPIIs have larger molecular weights (500-900 Da) than traditional small molecules (*132*). To that extent we tried screening the $G\alpha_q$-GRK2 interaction

against a collection of novel natural product extracts, however, the collection suffers heavily from artifacts when used in FCPIA.

Our FCPIA HTS campaign routinely yielded Z-factors between 0.8-0.9 (Figure 20B), indicating that our assay is well suited for HTS. Our results do indicate, however, that FCPIA suffers from a relatively high false positive hit rate that could be due to several factors. First, the assay is fluorescence based, and hence, will therefore suffer spectral artifacts that are common in many screening libraries. However, spectral artifacts are easily eliminated by the use of a fluorescent counter-screen, such as biotin/AF-$G\alpha_q$, and should therefore not be too concerning. Another assay artifact we discovered is chelation of aluminum. FCPIA uses 20 μM $AlCl_3$ in the assay buffer to form $GDP{\cdot}AlF_4^-$, which activates $G\alpha_q$ and allows it to bind to GRK2. We indentified a group of 12 compounds that contain 8-hydroxyquinoline, which is a chemical that can be used to chelate aluminum and measure its concentrations in water based on changes in its fluorescent spectra (*156-159*). Therefore, these compounds are most likely inhibiting the $G\alpha_q$-GRK2 interaction by deactiviating $G\alpha_q$ by removing the $GDP{\cdot}AlF_4^-$ complex.

Another reason our false positive hit rate appears high is due to the triage criteria that we used to select compounds for dose-response titrations. Overall, our HTS suffered from an overall lack of “hits”. Only 7 compounds had a percent inhibition by plate of greater than or equal to 50%. Comparatively, a similar assay (GRK2-

aptamer, see Chapter 5) yielded 144 compounds with percent inhibition by plate of greater than or equal to 50%. Thus, when we selected compounds for dose-response titrations we were dipping into the noise of the assay and thereby increasing our false positive hit rate.

Our initial search for discovering a small molecule inhibitor of $G\alpha_q$-GRK2 failed with no discernable lead compounds to test in secondary assays. While there appears to be a shallow pocket on GRK2 where residues 261-263 of $G\alpha_q$ bind (Figure 18B), it is still difficult to speculate if the surface of GRK2 can be targeted by small molecule inhibitors. Recently, a small molecule inhibitor of RGS4 was discovered that is believed to target an allosteric site on the RGS domain (*145*). It is intriguing to speculate if GRK2-$G\alpha_q$ could be modulated by a similar interaction, but this would likely require screening against larger libraries and compounds more selectively engineered to the defeat of PPI's, such as the natural products collections.

FUTURE DIRECTIONS

The $G\alpha_q$-GRK2 interaction is certainly a novel interaction, and the discovery of a small molecule inhibitor of the interaction would not only serve as a useful pharmacological tool, but it would also support the protein-protein interaction inhibitor movement. Our current HTS protocol is overall well suited for HTS, although, modifications to the assay could render the assay more useful by eliminating false positive hits due to aluminum chelation. A "simple" change is to

remove aluminum from the assay, and use GTPγS or GMPPnP to active the Gα subunit. However, loading $G\alpha_q$ with GTP is generally more challenging than the other Gα subunits due to the slower rate of GDP release. Our lab (and others) has been able to purify the non-receptor GEF Ric-8A and use Ric-8A to catalyze the exchange of GMPPnP onto $G\alpha_q$. This technique requires more protein, but given recent advances in our protein production capabilities and the fact the FCPIA uses so little protein, this is not a huge concern. We have already shown that GMPPnP loaded $G\alpha_q$ is capable of binding GRK2 (Figure 24A) and it would be interesting to see what effect our aluminum chelator inhibitors have on this interaction.

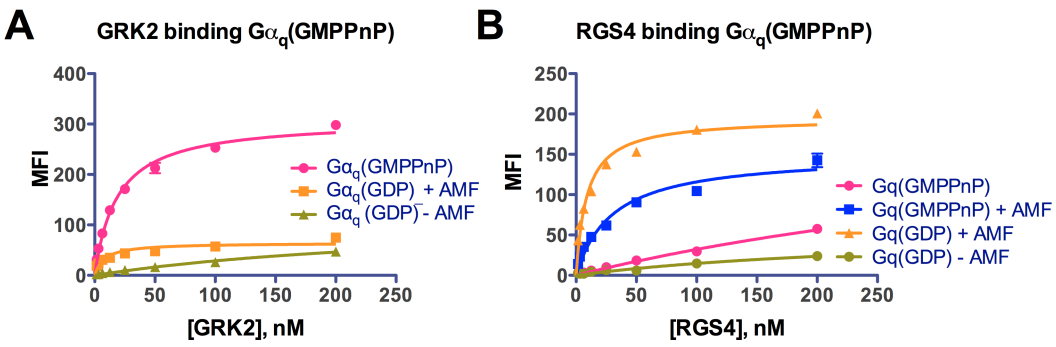

Figure 24: FCPIA with GMPPnP loaded $G\alpha_q$. **A)** GRK2 binding to $G\alpha_q$(GMPPnP). **B)** Loss of RGS4 binding affinity for $G\alpha_q$(GMPPnP). GMPPnP loaded $G\alpha_q$ could potentially eliminate many of the false positive hits seen in the $G\alpha_q$-GRK2 screen. The results show mean ± SEM run in duplicate.

Additional future directions could be aimed at generating small 3-4 amino acid peptides of either GRK2 or $G\alpha_q$. Such peptides could be used in an FP assay to

increase throughput over FCPIA and allow for screening at larger screening centers. More importantly, if such peptides are able to inhibit the $G\alpha_q$-GRK2 interaction, they themselves could be used a starting point for a more rational design of small molecules that mimic the properties of the peptide (*167*).

Chapter 4
Molecular Mechanism of Selectivity Among GRK2 Inhibitors

BACKGROUND AND RESEARCH PLAN

Dysregulation of kinase mediated signaling pathways results in a vast number of diseases including cancer, inflammation, diabetes, and heart failure, making them excellent targets for therapeutic intervention. The kinase domain is composed of two lobes connected by a hinge region, with ATP binding between the two lobes (Figure 25). There are several critical structural elements that cluster around the ATP binding sites of these kinases, including a phosphate-binding loop (P-loop), an αC helix, a hinge loop, and an activation loop. Differences in these structures among the ~500 kinases in the human genome have generally been the focus for the rational design of selective kinase inhibitors and have underlain the molecular basis for selectivity exhibited by known inhibitors (*168-172*).

Since the discovery of the linkage between the overexpression of GRK2 and heart failure, GRK2 has been considered a pharmaceutical target for the treatment of cardiovascular disease (see Chapter 5) (*173*). Structural analysis of bovine GRK2 has led to several crystal structures including complexes with the heterotrimeric G proteins $G\alpha_q$ and $G\beta\gamma$, and the non-selective AGC kinase

inhibitor balanol (Figure 26) (*26, 174, 175*). Comparison of the ligand free GRK2 structure with the balanol bound structure revealed that balanol stabilizes a slightly more closed conformation of the kinase domain (4° closure of large relative to small lobe). However, an additional 16° rotation of the large lobe is still required to achieve the fully closed state, thus, balanol appears to stabilize a distinct inactive (open) conformation of GRK2 (*175*).

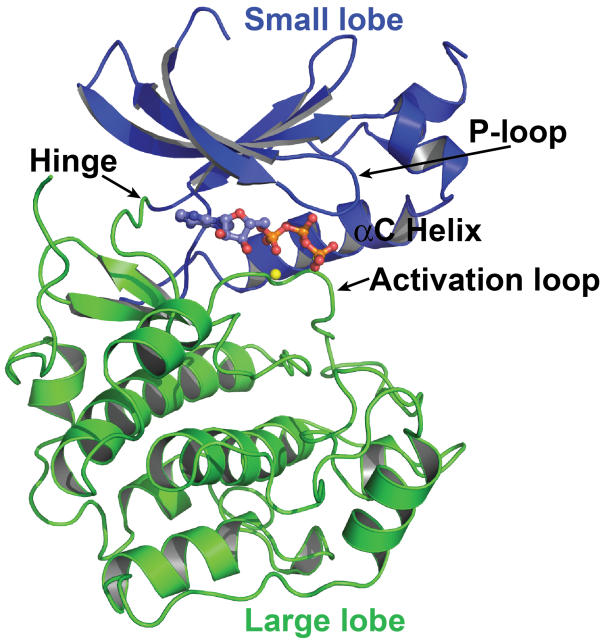

Figure 25: Structure of the catalytic domain of GRK2. The small (N-terminal) lobe (blue), consists of a β sheet, a phosphate binding loop (P-loop), and an αC helix that bears catalytic residues. The large (C-terminal) lobe (green), is primarily helical and contains an activation loop that in most protein kinases is phosphorylated in order to achieve full activity (GRKs lack this phosphorylation site). ATP binds between the two lobes, which are connected by a short hinge.

ATP is modeled from the crystal structure of the GRK1·ATP complex (PDB: 3C4W).

Recently, a class of heterocyclic compounds has been discovered by Takeda Pharmaceuticals (*176*) that both selectively inhibit GRK2 and show therapeutic potential (Figure 27). In an effort to visualize GRK2 in a new, hopefully more active conformation, and to determine the mechanism of selectivity for these inhibitors, we proceeded to co-crystallize two of the discovered compounds (CMPDs 1/2, Figure 27) with the GRK2-Gβγ complex. The solved crystal structures suggested that residues in the P-loop and αB-αC helices could contribute to compound selectivity. Mutagenesis studies were performed to convert non-conserved residues around the inhibitor-binding site in an attempt to alter compound selectivity between GRK2 and GRK1, however with only modest success. Therefore, the relative degree of kinase domain closure of GRK2 relative to other GRKs may dictate selectivity for these compounds.

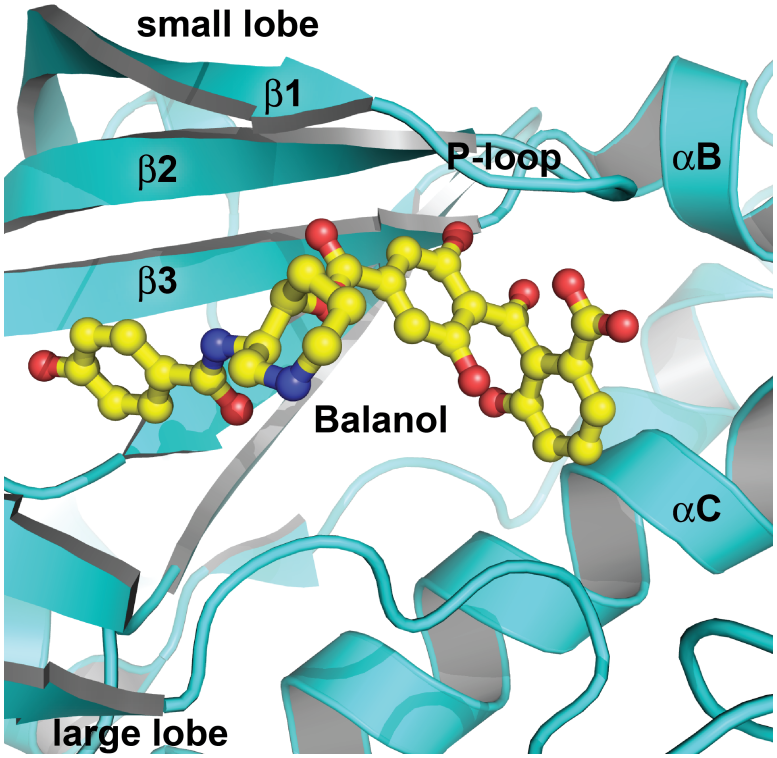

Figure 26: Crystal structure of the hGRK2·balanol-Gβγ complex. Balanol bound to the ATP-binding site of human GRK2 (hGRK2) (PDB: 3KRW). Balanol is drawn as a ball and stick model with carbons colored yellow, nitrogens blue, and oxygens red. Conformational changes are observed in the P-loop and αB-αC helices of the small lobe as a consequence of binding.

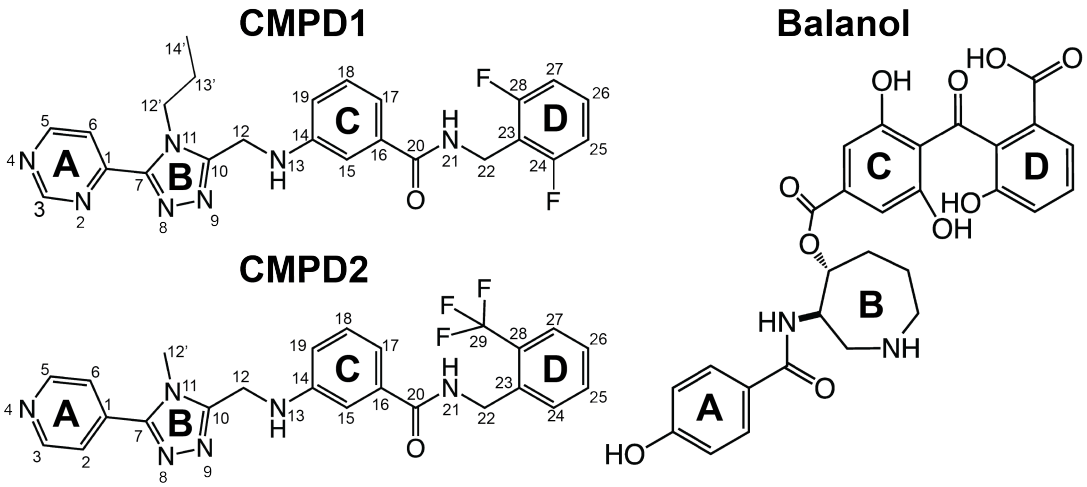

Figure 27: Small molecule inhibitors of GRK2. The chemical structures of compounds (CMPD) 1, 2, and balanol. CMPD's 1/2 are potential cardiotonic drugs discovered by Takeda Pharmaceutical Company (*176*). Balanol is a non-specific AGC kinase inhibitor that is a natural product from the fungus *Verticillium balanoides (177)*. The ring structures are labeled as follows for CMPD's 1/2: **A** = pyrimidine / pyridine, **B** = substituted 1,2,4-triazole, **C** = aminobenzamide, **D** = substituted benzene; for Balanol: **A** = p-hydroxybenzamide, **B** = azepane, **C**&**D** = substituted and esterified benzophenones.

METHODS

Reagents

Compound 1 (CMPD1), and compound 2 (CMPD2) were synthesized by an outside firm, and compounds were aliquoted and stored in 100% DMSO at -20°C. Balanol was obtained from a natural source as described previously (*175*).

Purification of GRK2

GRK2 was expressed from a baculovirus vector containing the cDNA for bovine GRK2-S670A with an engineered C-terminal hexahistidine tag (*178*). For protein expression, 25 mL of GRK2 baculovirus was added per 750 mL of High 5 cells at density of approximately $4x10^6$ cells/mL. The cells were harvested after 36-40 hours and all purification steps were performed at 4 °C. Cell pellets were thawed and resuspended in lysis buffer containing 20 mM HEPES pH 8.0, 50 mM NaCl, 10 mM β-mercaptoethanol (βME), and protease inhibitors (1 mM PMSF, 1 μM leupeptin, and 1 mM lima bean trypsin inhibitor). Cells were homogenized with a dounce and lysed using a C3 Avestin homogenizer (~10,000 psi). The lysed cells were separated by ultracentrifugation using a Beckman Ti-45 rotor at 45,000 rpm for 60 min. The supernatant was collected, filtered, and diluted to a concentration of ~5 mg/mL in lysis buffer. The filtered supernatant was then loaded onto a 10 mL nickel NTA column pre-equilibrated with lysis buffer. The column was washed with 200 mL of lysis buffer, followed by 200 mL of lysis buffer supplemented with 150 mM NaCl and 20 mM imidazole. The protein was then eluted with 100 mL lysis buffer plus 150 mM imidazole and collected in 10 mL fractions. Fractions containing protein were identified via mini-Bradford assay, pooled and then diluted 5-fold into 20 mM HEPES pH 8.0 and 2 mM dithiothreitol (DTT). The diluted protein was filtered and loaded onto an 8 mL Source 15 S column (GE Healthcare). Protein was eluted off with an 80 mL salt gradient from 0 to 500 mM NaCl and GRK2 containing fractions were confirmed via SDS-PAGE (Figure 28). The protein was then concentrated with an Amicon

Ultra 50 kDa to a concentration of ~10 mg/mL. The protein was then either frozen in liquid nitrogen for storage or loaded onto two tandem S200 gel-filtration columns (GE Healthcare) pre-equilibrated with 20 mM HEPES pH 8.0, 200 mM NaCl, and 2 mM DTT. Peak fractions were analyzed by SDS-PAGE, pooled, and concentrated with an Amicon Ultra 50 kDa to ~10 mg/mL. This protocol generally produced 10 mg of purified GRK2 from 6 L of culture.

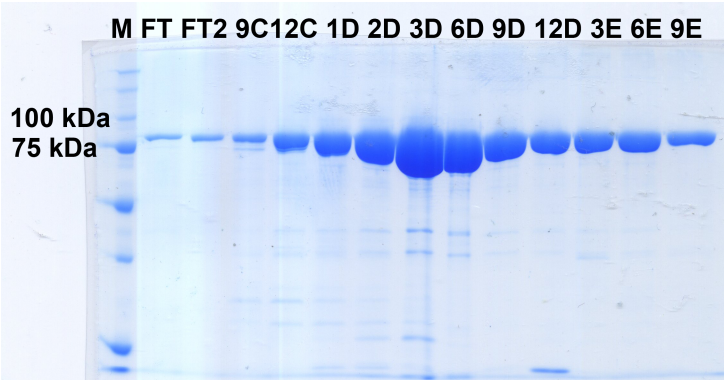

Figure 28: Purification of GRK2. SDS-PAGE of GRK2 containing fractions eluted off an 8 mL Source 15S column (GE Healthcare). Fractions 1D-11E were pooled and concentrated.

Purification of Gβγ

A pellet of cells expressing wild type $G\beta_1\gamma_2$-H_6 (Gβγ) (harvested on 2-20-09) was provided by V. Tesmer. Cells were resuspended in 200 mL of lysis buffer containg: 20 mM HEPES pH 8.0, 100 mM NaCl, 10 mM βME, 0.1 mM EDTA, and protease inhibitors (LL+PMSF). Cells were homogenized with a dounce and lysis was performed by sonication. The insoluble, membrane pellet was isolated via ultracentrifugation using a Ti 45 at 45,000 rpm for 1 hour, and then resuspended,

homogenized, and brought to a final volume of 400 mL with lysis buffer at a concentration of ~ 10 mg/mL. Sodium cholate was added to 1% w/v and stirred in a beaker at 4 °C for 1 hour. The supernatant was then isolated using a second ultracentrifugation step. The supernatant was diluted into an equal volume of buffer (Buffer A) containing: 20 mM HEPES pH 8.0, 100 mM NaCl, 1 mM $MgCl_2$, and 10 mM βME and then loaded onto a 5 mL nickel NTA column. The nickel column was washed with 50 mL of buffer A containing 0.2% sodium cholate, and then washed with 100 mL of buffer A containing 300 mM NaCl, 10 mM imidazole, and 10 mM CHAPS. The protein was eluted with 25 mL of buffer A containing 10 mM CHAPS and 200 mM imidazole, and then diluted into 75 mL of buffer A containing 0 mM NaCl. Protein was then filtered and loaded onto Mono Q column containing buffer A (with no salt). Gβγ was eluted with a 20 mL salt gradient, and Gβγ-containing fractions (0.5 mL) were confirmed via SDS-PAGE (Figure 29A). Gβγ was then pooled and concentrated with a Centricon 50 kDa to ~10 mg/mL, and further purified over tandem S200 gel filtration columns and concentrated to 10 mg/mL (Figure 29B).

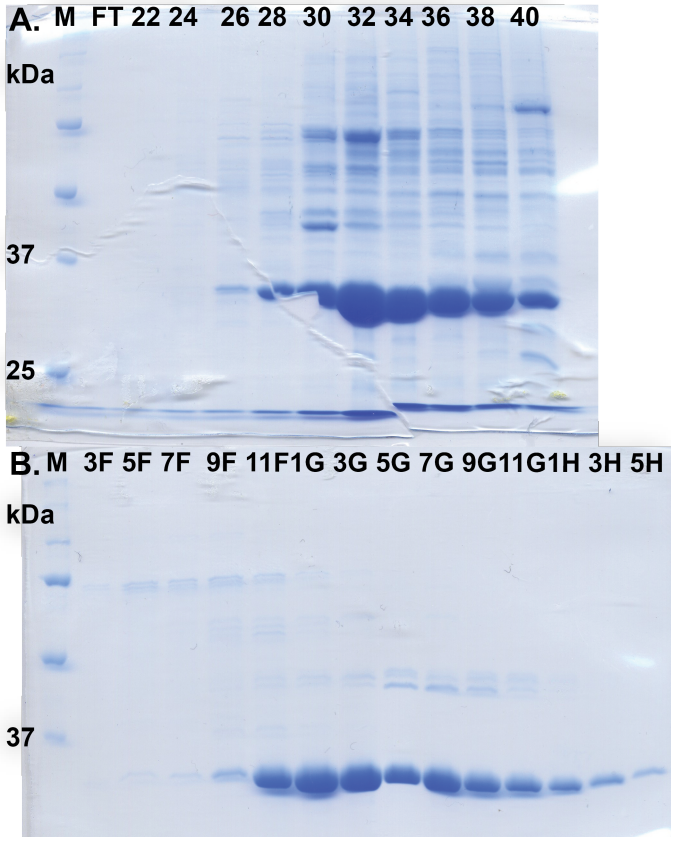

Figure 29: Purification of Gβγ. A) SDS-PAGE of Gβγ following separation by Mono Q anion exchange chromatography. Fractions 28-40 were pooled. **B)** SDS-PAGE of Gβγ fractions following gel filtration. Fractions 9F-3H were pooled.

Purification of the GRK2-Gβγ Complex

The GRK2-Gβγ complex was formed by mixing purified bovine GRK2-S670A (200 μL, 2.14 mg) with purified Gβγ (200 μL, 1.6 mg) and then supplementing with additional CHAPS and $MgCl_2$ to final concentrations of 10 mM and 5 mM, respectively. The protein mixture was incubated on ice for 30-60 minutes, and then filtered and loaded onto two tandem S200 gel filtration columns. Formation of the complex was verified by SDS-PAGE (Figure 30), and the GRK2-Gβγ

containing fractions were pooled and concentrated (Amicon Ultra 50 kDa) to a final concentration of 13 mg/mL (*100*).

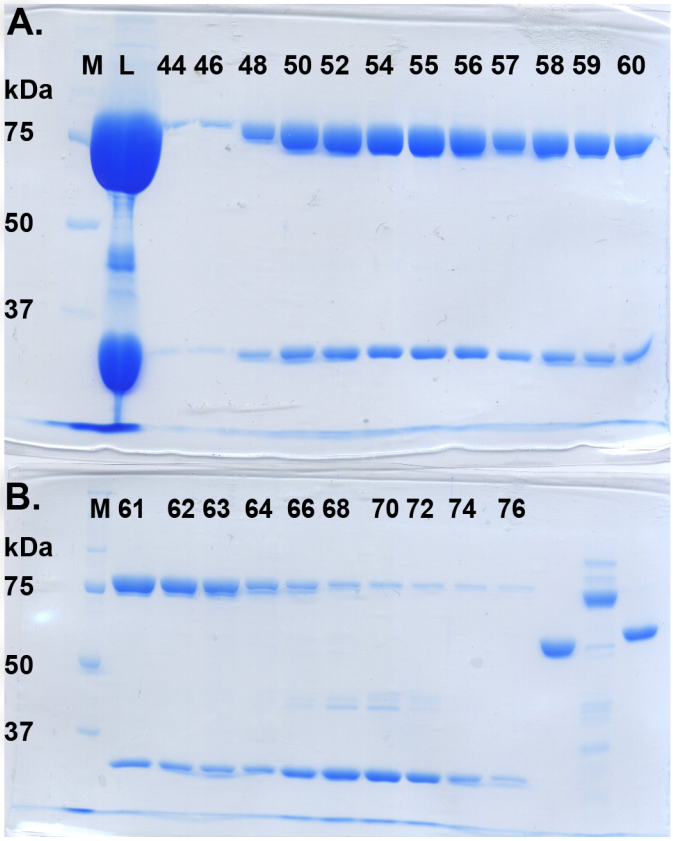

Figure 30: Purification of the GRK2-Gβγ complex. A) Peak fractions 44-60 and **B)** 61-76 from a GRK2-Gβγ gel filtration run. Fractions #48-62 were pooled and concentrated to 13 mg/mL. Fractions past 62 contained excess Gβγ and were not used.

Crystallization of Ligand Bound GRK2-Gβγ Complex

Initially we attempted to co-crystallize GRK2 alone with CMPDs 1/2, however, those attempts yielded no crystal leads. We then sought to co-crystallize

CMPD's 1/2 with GRK2-Gβγ using previously determined crystallization conditions for GRK2-Gβγ (*179*). Initial trays were set up by adding either 100 μM CMPD1, 100 μM CMPD2, or 1 mM ATP to the concentrated GRK2-Gβγ complex on ice for 30 minutes. Crystals were grown at 4°C by hanging drop vapor diffusion method initially with the protein mixed with the well solution at 1μL to 1μL ratio, and were observable after 1 day (Figure 31). Many different well conditions generated crystals such as: 100-200 mM NaCl, MES pH 5.6-6.7, and 5-8% PEG 3350. The best diffraction data for a GRK2·CMPD1-Gβγ crystal was harvested from a well solution containing 7% PEG3350, MES pH 6.25, 250 mM NaCl with drops composed of 2μL protein (10mg/mL protein) mixed with 2μL well solution. Likewise, the best crystal for GRK2·CMPD2-Gβγ was harvested from 7% PEG3350, 200 mM NaCl, and MES pH 5.25 with drops composed of 2 μL protein (10 mg/mL protein) mixed with 2 μL well solution. For comparison, GRK2·ATP-Gβγ crystals were also generated using well solution with 9% PEG 3350, 200 mM NaCl, and MES pH 6.5 with 1μL:1μL drops. All crystals were harvested into a cryoprotectant solution containing: 20 mM HEPES pH 8.0, 100 mM MES (at the well solution pH), 300 mm NaCl, 10 mM CHAPS, 5 mM $MgCl_2$, 2 mM DTT, 9% PEG3350, 25% ethylene glycol, and either 100 μM CMPD1/2 (in 100% DMSO, final concentration 2% DMSO) or 1 mM ATP. 2% DMSO was added to the harvesting solution for the GRK2·ATP-Gβγ crystals so they would be equivalent to the CMPD1/2 crystal harvesting solutions.

The inhibitor bound GRK2-Gβγ complexes crystallized in the space group C2 and diffracted anisotropically to spacings beyond 2.5 Å at APS beamline 21-ID-G. Overall, two complete data sets were collected for CMPD1, five for CMPD2, and two for ATP, and the data sets that produced the best omit maps with the highest redundancy were used for the structure determination. The structures were solved using molecular replacement with the original GRK2-Gβγ structure (PDB: 1OMW) (*174*) as the starting model (REFMAC5). Models for the ligands were generated using Sketcher (CCP4 6.1) and PRODRG (*180*) (http://davapc1.bioch.dundee.ac.uk/prodrg/). The ligand bound GRK2-Gβγ models were built using COOT (*181*), and refined using TLS and restrained refinement in REFMAC5 (*182, 183*). MOLPROBITY (*184*) and PROCHECK (*185*) were used for structure validation.

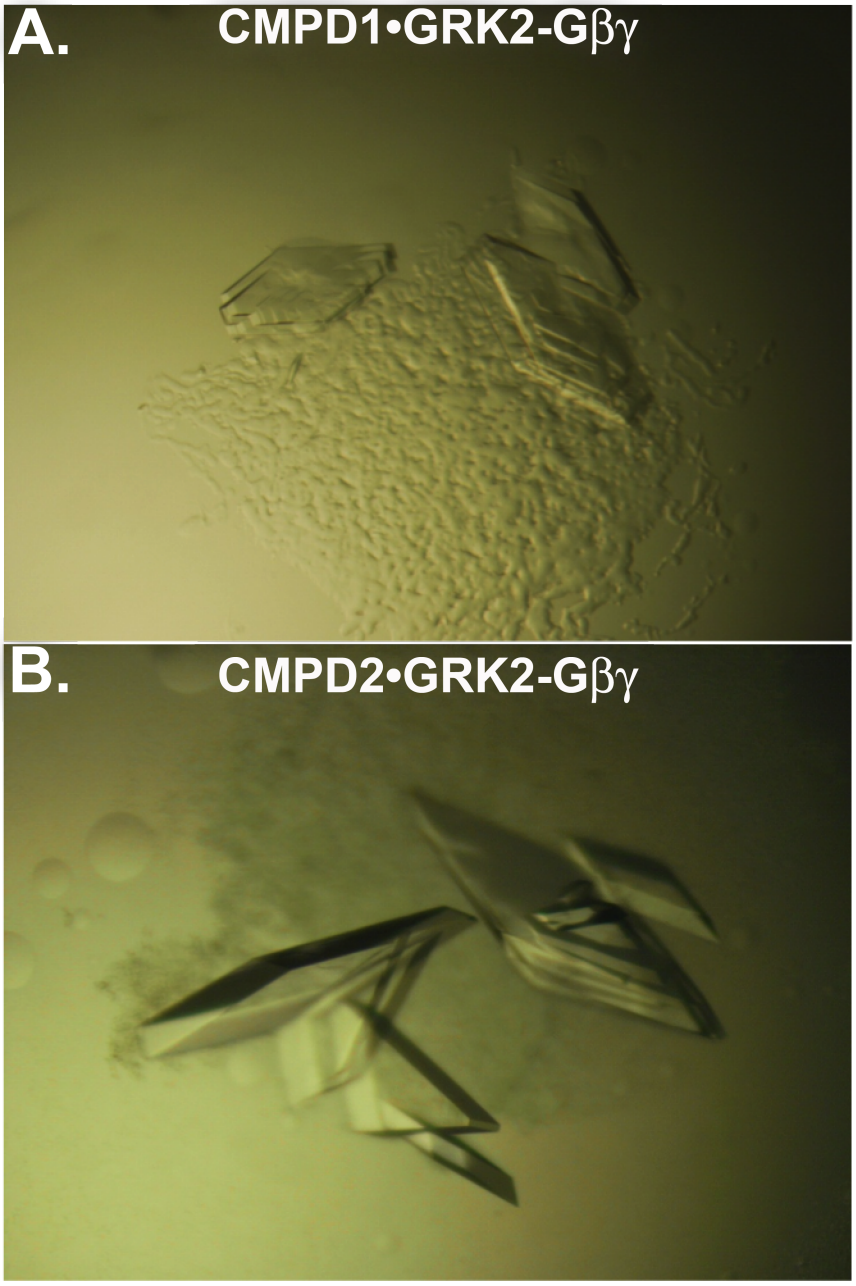

Figure 31: Crystallization of GRK2·CMPD1/2-Gβγ. Crystals of **(A)** CMPD1•GRK2-Gβγ and **(B)** CMPD2•GRK2-Gβγ. Crystals reached a maximum size of approximately 420 x 140 x 70 μm. Both crystals belong to the space group C2.

Production of GRK2, GRK1, and GRK5 Mutants

GRK2 mutants were made using the QuickChange site-directed mutagenesis kit (Stratagene) to introduce mutations into the GRK2-H_6 construct. Mutants were expressed and purified as described for GRK2. A baculovirus construct expressing bovine GRK1 with a C-terminal truncation at residue 535 and a hexahistidine tag ($GRK1_{535}$-H_6) was used to express GRK1 and the protein was purified as previously described (*186*). GRK5 with a C-terminal truncation at residue 561 followed by a hexahistidine tag ($GRK5_{561}$-H_6) was expressed using a vector generated by Dr. Chih-chin Huang and purified similarly to $GRK1_{535}$-H_6 (*178*).

Rhodopsin Phosphorylation Assays

Urea-washed bovine rod outer segments (bROS) were purified as previously described (*187*). Steady-state kinetics were conducted using saturating concentrations of ATP (0.5 mM ATP + [γ^{32}P-ATP]), 5-20 μM bROS, and 50 nM GRK in a buffer containing: 20 mM HEPES pH 8.0, 1 mM CHAPS, 5 mM $MgCl_2$, and 2 mM DTT. The reactions were carried out in a 96-well PCR plate. For inhibition assays, 5 μL of varying concentrations of compound were added to each well, followed by addition of 5 μL GRK, and then 5 μL of bROS (added in the dark). The plate was then allowed to equilibrate for at least 30 minutes. The reaction was initiated by the addition of 5 μL of ATP and exposure to light at room temperature (~25°C). The reaction was quenched after 5-10 minutes (within the linear range of enzyme activity, Figure 32) with the addition of 4 μL of

SDS-PAGE loading buffer. Reactions were then analyzed by SDS-PAGE. The gels were dried and exposed to a phosphor-imaging screen, and phosphorylated rhodopsin was quantified using a Typhoon 9410 imager (GE Healthcare).

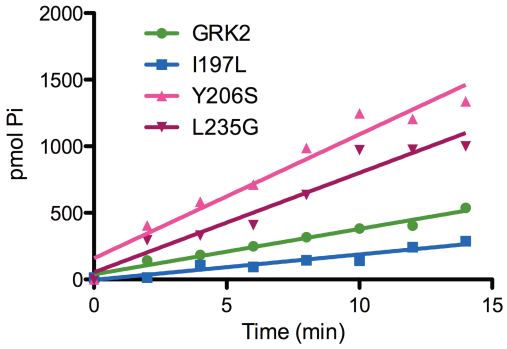

Figure 32: Linear kinetics of GRK2 activity. Phosphorylation of bROS by GRK2 and the GRK2 mutants I197L, Y206S, and L235 over a time course of 15 min. Subsequent single time point phosphorylation assays were performed in the linear range of GRK2 activity (5 or 10 min time point).

Enzyme activity was calculated as follows: for 500 μM ATP, the reactions contain 500 pmoles of ATP per one μL. One μL of reaction is diluted 1:1000 in assay buffer and one μL of the dilution is spotted onto the dried gels in multiple replicates (ATP-standard). The ATP-standard is then calculated by dividing the amount of ATP (0.5 pmoles) by the averaged volume (from the phospho-imager). Sample reaction volumes are then multiplied by the ATP-standard to yield pmoles of P_i, which is then corrected by a dilution factor to yield total pmoles of P_i. The total pmoles of P_i per sample is divided by reaction time (in minutes) and